Chapter II

Effect of High Electric Fields on the N-I Phase Transition of a Nematic Liquid Crystal Exhibiting Large Negative Dielectric Anisotropy

2.1 Introduction

Studies on the effects of electric and magnetic fields on liquid crystals are interesting both from fundamental and technological points of view. There have been several reports on the effect of *strong* electric and magnetic fields on the isotropic to nematic phase transition [1-7]. The electric field experiments were performed on systems exhibiting positive dielectric anisotropy ($\Delta\varepsilon = (\varepsilon_{\parallel} - \varepsilon_{\perp}) > 0$), where the subscripts refer to directions in relation to $\hat{n}$. The free energy density due to the electric field is given by

$$F_e = -\frac{1}{8\pi}\varepsilon_{\parallel}E^2\cos^2\theta - \frac{1}{8\pi}\varepsilon_{\perp}E^2\sin^2\theta \qquad (2.1)$$

where $\varepsilon_{\parallel}$ and $\varepsilon_{\perp}$ are the principal dielectric constants, E the applied electric field and θ is the angle between the director and the electric field (Fig.(2.1)). Equation (2.1) can be rewritten as

$$F_e = -\frac{1}{8\pi}\Delta\varepsilon\left(\hat{n}.\vec{E}\right)^2 - \frac{1}{8\pi}\varepsilon_{\perp}E^2 . \qquad (2.2)$$

It is seen that for a material with $\Delta\varepsilon$ >0, the free energy density is reduced when the director is parallel to the electric field while for a material with $\Delta\varepsilon$ < 0, the free energy density is reduced when the director is perpendicular to the field. For a material with $\Delta\varepsilon > 0$, at high fields,

$$F_e = -\frac{1}{8\pi}\varepsilon_{\parallel}E^2 . \qquad (2.3)$$

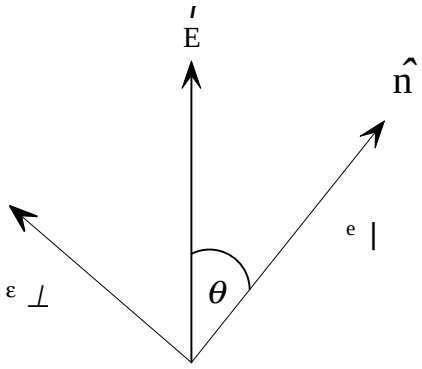

Figure 2.1: Schematic diagram showing the direction of the field with respect to the director.

The free energy density can be lowered with the field if $\varepsilon_{\parallel}$ is enhanced. Consequently the distribution function is enhanced near the director. Thus S is increased and $\varepsilon_{\perp}$ is decreased under field. Expressing $\varepsilon_{\parallel}$ in terms of S we can write

$$\varepsilon_{\parallel} = \bar{\varepsilon} + \frac{2}{3}\Delta\varepsilon_0 S \tag{2.4}$$

where $\bar{\varepsilon} = \left(\varepsilon_{\parallel} + 2\varepsilon_{\perp}\right)/3$ is the average dielectric constant and S is the orientational order parameter, given by

$$S = \frac{\Delta\varepsilon}{\Delta\varepsilon_0} \tag{2.5}$$

where $\Delta\varepsilon_0$ is the anisotropy in the fully aligned state (S=1) [8]. In the presence of field, the order dependent part of equation (2.3) can be written as

$$F_e = -\frac{\Delta\varepsilon_0 S E^2}{12\pi}. \tag{2.6}$$

Thus application of a strong electric field to nematic liquid crystal with $\Delta\varepsilon > 0$ leads to an enhancement of orientational order parameter [4]. A strong field also shifts the paranematic-nematic transition temperature (T_{PN}). For a field to shift T_{PN} by a measurable amount, the field energy should be comparable to the thermal energy $k_B T$. Similar effects on nematic liquid crystal can also be seen under a magnetic field. The volume

diamagnetic anisotropy ($\Delta\chi$) of a typical nematic is ~10^{-7} cgs units and the *molecular* diamagnetic anisotropy $\Delta\chi_m$ is given by

$$\Delta\chi_m = \frac{\Delta\chi}{N} \tag{2.7}$$

where *N* is the number of molecules per unit volume. The number density is given by

$$N = \frac{N_A \rho}{M} \tag{2.8}$$

where ρ is the density of the medium, $N_A \approx 6.02\times10^{23}$ /mole is the Avogadro number and *M*, the molecular weight. Assuming M = 300, ρ =1 *gm/cc*, we get $\Delta\chi_m$ ~10^{-29} *cgs* units. The anisotropic part of the magnetic energy per molecule is given by

$$F_m = \frac{-\Delta\chi_m H^2}{2}. \tag{2.9}$$

The required field energy to be equal to the thermal energy (at T = 300*K*), H should be ~ 10^7 gauss. So far only a magnetic field of ~10^5 gauss has been applied to thermotropic liquid crystals producing a very small shift in the paranematic-nematic transition temperature (~6mk) [7]. On the other hand the dielectric anisotropy (~20) can be much larger than diamagnetic anisotropy. Making a similar calculation as above, but replacing $\Delta\chi$ by $\Delta\varepsilon/4\pi$ and H by E one finds that the required electric field is ~10^5 V/cm (~300 esu). This electric field is practically attainable in the laboratory.

In this chapter we will describe the first experiment on the effect of strong electric field on the paranematic-nematic transition on a system with negative dielectric anisotropy to find some interesting results. First we give the theoretical background for describing the nematic-isotropic phase transition in the absence as well as in the presence of electric field.

2.2 Theoretical Background

2.2.1 Landau Theory of Phase Transitions

The Landau theory is a phenomenological theory, which was developed for describing second order phase transitions. In such a phase transition the order parameter increases continuously across the transition point, and close to the transition point the

order parameter is very small. Therefore the free energy density F can be expanded in powers of order parameter S which characterises the lower symmetry phase [9].

$$F(p,T,S) = F_0 + \frac{A}{2}S^2 + \frac{C}{4}S^4 \tag{2.10}$$

where F_0 is the free energy density of the disordered phase ($S = 0$). The absence of the linear term in S in equation (2.10) ensures the stability of the higher temperature phase. In the ordered phase ($S \neq 0$), the minimum in F is ensured by assuming $A < 0$ and in the disordered phase ($S = 0$) the minimum in F is ensured by assuming $A > 0$. Landau assumed that $A = a(T-T^*)$ where a is a constant and T^* is the transition temperature and C (>0) is a constant which does not depend on temperature. Equation (2.10) is valid for a system in which the free energy density is independent of the sign of order parameter S (e.g. ferromagnetic system) i.e. $F(S) = F(-S)$ and the cubic and the higher odd powers of S are not allowed. Therefore the free energy density can be written as

$$F(p,T,S) = F_0 + \frac{a}{2}\left(T - T^*\right) S^2 + \frac{C}{4}S^4 . \tag{2.11}$$

The equilibrium value of the order parameter is found by using $F' = 0$ and $F'' > 0$ (each prime denotes a differentiation with respect to S)

$$S = \left[a\frac{\left(T - T^*\right)}{C} \right]^{\frac{1}{2}} . \tag{2.12}$$

The order parameter profile is continuous with temperature for the second order phase transition.

2.2.2 Landau-de Gennes Theory for the Nematic to Isotropic (N-I) Phase Transition

As we have discussed in section 1.2.1 the orientational order parameter of nematic liquid crystal is defined as $S = \frac{1}{2}\left\langle 3\cos^2\theta - 1 \right\rangle$ where θ is the angle between the long axes of the molecules and the director. The order parameter S can take any value between –1/2 to 1. The two extreme values of S describe two distinct physical situations of the system. The first one corresponds to a situation with $\theta = \pi/2$ and second one to $\theta = 0$. The positive and negative values of S arise in general from different distribution

functions, hence $F(S) \neq F(-S)$. Hence the free energy density of the nematic phase must include the cubic power of S and is given by

$$F(p,T,S) = F_0 + \frac{a}{2}(T - T^*) S^2 - \frac{B}{3}S^3 + \frac{C}{4}S^4 \qquad (2.13)$$

where T^* is the temperature below which the isotropic phase can not be supercooled and the negative sign of the cubic term has been assumed to get a lower free energy for $S > 0$. Minimising the above equation with respect to S we get two solutions

$$S = 0$$

and

$$S_{\pm} = \frac{B}{2C} \pm \frac{\sqrt{B^2 - 4aC(T - T^*)}}{2C}. \qquad (2.14)$$

$S = 0$ corresponds to the isotropic phase. S_+ corresponds to the lower minimum in the free energy in the stable nematic phase. The nematic-isotropic transition temperature T_{NI} can be calculated by equating the free energy density in the nematic phase to that of the isotropic phase i.e. $F(p,T,S) = F_0$, which gives

$$\frac{a}{2}(T_{NI} - T^*) S_{NI}^2 - \frac{B}{3}S_{NI}^3 + \frac{C}{4}S_{NI}^4 = 0 \qquad (2.15)$$

where S_{NI} is the order parameter at the transition point. The equilibrium condition yields

$$a(T_{NI} - T^*) S_{NI} - BS_{NI}^2 + CS_{NI}^3 = 0. \qquad (2.16)$$

From equations (2.15) and (2.16), we get

$$S_{NI} = \frac{2B}{3C},$$

and

$$T_{NI} = T^* + \frac{2B^2}{9aC} \qquad (2.17)$$

Equation (2.14) has a real solution only when $B^2 - 4Ca(T - T^*) > 0$, leading to an upper temperature limit above which the nematic phase cannot exist. This temperature T^{**} is given by

$$T^{**} = T^* + \frac{B^2}{4Ca}. \qquad (2.18)$$

The variation of the free energy density as a function of order parameter for various temperatures is shown in Fig.(2.2). When $T > T^{**}$ there is only one minimum in

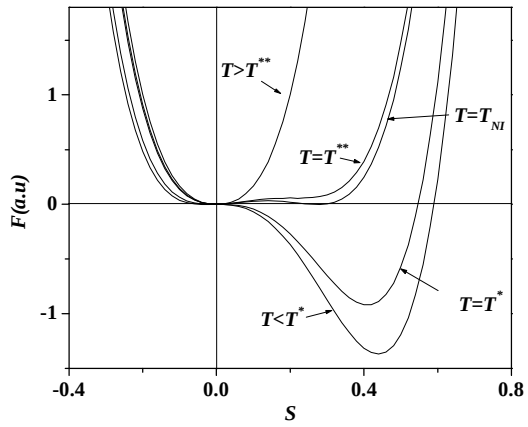

Figure 2.2: Variation of the free energy density as a function of order parameter at various temperatures near nematic–isotropic transition. For $T<T^*$ there is a second minimum in F at S = -0.02 which is hardly visible.

the free energy curve corresponding to $S=0$, i.e. the isotropic phase. An inflection is observed in the free energy density curve at $T=T^{**}$. For $T_{NI} < T < T^{**}$ there are two minima one of which corresponds to the isotropic phase ($S=0$) and other one corresponds to the superheated nematic phase. At $T=T_{NI}$ there are two minima of equal energy density. Therefore a first order phase transition takes place from $S=0$ to $S=S_{NI}$. For $T^* < T < T_{NI}$ there are again two minima, the absolute minimum corresponds to the nematic phase. Below T^* the isotropic phase can not be supercooled. At $T=T^*$ there is only one minimum corresponding to $S > S_{NI}$ and an inflection point at S=0. For $T < T^*$, there is a second minimum for a negative value of S, and the corresponding energy is higher than that for S >0. The inclusion of third order term explains the first order phase transition seen in all nematogens. The corresponding jump in the order parameter is ~0.3.

2.2.3 Nematic-Paranematic Phase Transition in the Presence of an External Electric Field for a System with $\Delta\varepsilon > 0$

As explained earlier (equation (2.6)) in the presence of an external field a linear term in S has to be added in the Landau free energy expansion (equation (2.13)). This prevents the existence of the isotropic phase. The field induces a weak orientational order even in the higher temperature phase, as a result of which all the physical properties in

the medium become weakly anisotropic (*paranematic phase*). The field-induced birefringence in the paranemati*c* phase due to the electric field is called the Kerr effect, and the analogous effect due to a magnetic field is called the Cotton-Moutton effect. The free energy density in the presence of the electric field can be written as

$$F(p,T,S) = F_0(p,T) - hS + \frac{a(T-T^*)}{2}S^2 - \frac{B}{3}S^3 + \frac{C}{4}S^4 \qquad (2.19)$$

where $h = \frac{\Delta\varepsilon_0}{12\pi}E^2$. Minimising equation (2.19) with respect *S* we get

$$a(T-T^*) = \frac{h}{S} + BS - CS^2 . \qquad (2.20)$$

It is seen that when the field is switched on, a given value of *S* occurs at a higher temperature. The variation of the free energy density in the presence as well as in the absence of field is shown for a system with $\Delta\varepsilon > 0$ in Fig.(2.3) for $T > T_{NI}$. The electric field phase diagram is shown in Fig.(2.4). It is seen that under an electric field the paranematic to nematic transition temperature is shifted to the higher value and the order parameter is increased in the nematic phase. At low fields the transition occurs with a finite jump in the order parameter in a first order phase transition.

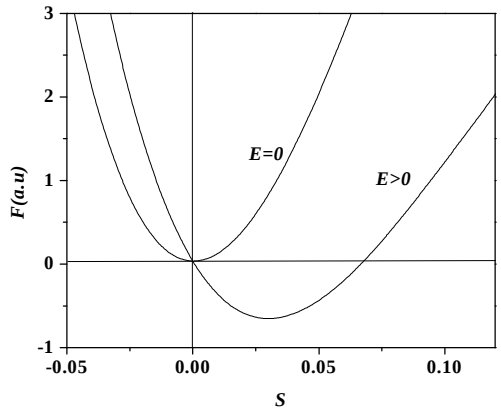

Figure 2.3: Variation of free energy density as a function of the order parameter in the presence and absence of an electric field for $T > T_{NI}$.

With increasing field the jump decreases and above a critical field there is a continuous evolution of the order parameter from the paranematic to nematic phase. These

phenomena resemble the classical gas to liquid transition under pressure. Since the symmetries of the two phases are the same the possibility of a second order phase transition can be ruled out except at the critical point. At the critical point $F' = F'' = F''' = 0$, where each prime denotes a differentiation with respect to *S*. Differentiating equation (2.19) thrice with respect to *S* and equating to 0, we obtain the following relations [10]

$$S_c = \frac{B}{3C}$$

$$T_c = T^* + \frac{B^2}{3aC}$$

$$E_c^2 = \frac{4\pi B S_c^2}{\Delta\varepsilon_0} \tag{2.21}$$

where S_c, T_c and E_c are the critical values of the order parameter, temperature and corresponding electric field respectively. The shift in the transition temperature is given by [1]

$$T_{PN}(E) - T_{NI}(0) = \left[\frac{T_{NI}(0)}{Q}\frac{\Delta\varepsilon}{12\pi}\right]E^2. \tag{2.22}$$

where ρ is the desnity, *Q* the latent heat of transition, given by $\frac{1}{2}aT_{NI}S_{NI}^2$ in the Landau de Gennes theory.

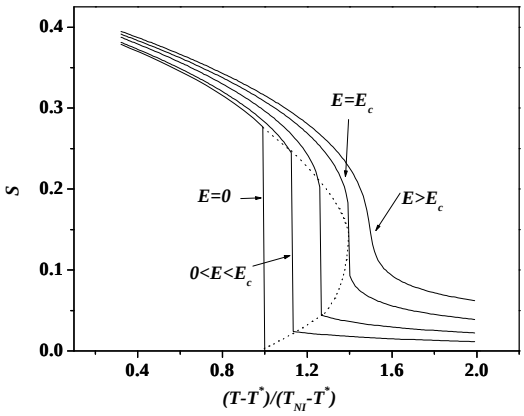

Figure 2.4: Theoretical variation of the order parameter as a function of reduced temperature at various electric fields. The dashed line indicates the coexistence region.

2.2.4 Macroscopic Quenching of Thermal Fluctuations of the Director

So far we have discussed the effect of a strong electric field on the N-I phase transition. In the nematic phase there are thermal fluctuations of the director, which introduce distortions of the director field. In chapter-I (Fig.(1.5)) the three types of distortion are shown pictorially. These fluctuations cause strong light scattering (10^6 times larger than the scattering from an isotropic fluid). As a result the nematic is turbid in appearance. It was pointed out by de Gennes [11] that a strong field could partially quench the director fluctuations and hence the order parameter can be enhanced. Suppose the average orientation of the director is along the *z*-axis. The fluctuation of the optic axis at any point '*r*' will be described by small non-zero components $n_x(r)$, $n_y(r)$. To second order in $n_x(r)$ and $n_y(r)$ the distortion energy density is given by [11]

$$F_d = \frac{1}{2}\left[K_1\left(\frac{\partial n_x}{\partial x} + \frac{\partial n_y}{\partial y} \right)^2 + K_2\left(\frac{\partial n_x}{\partial y} - \frac{\partial n_y}{\partial x} \right)^2 + K_3\left[\left(\frac{\partial n_x}{\partial z} \right)^2 + \left(\frac{\partial n_y}{\partial z} \right)^2 \right] \right] \tag{2.23a}$$

where K_1, K_2, K_3 , are the splay ,twist and bend elastic constants respectively. For simplicity, using the one constant approximation we can write the distortion energy density as

$$F_d = \frac{1}{2} K (\nabla n_\perp)^2 \tag{2.23b}$$

where $n_\perp$ is the fluctuation in a direction perpendicular to the *z*- axis. It is convenient to analyse $n_\perp$ in Fourier components

$$n_\perp(\vec{q}) = \frac{1}{V}\int n_\perp(\vec{r})\, e^{i\vec{q}.\vec{r}}\, d\vec{r} \,. \tag{2.24}$$

From equations (2.23b) and (2.24), we get

$$F(q) = \frac{1}{2} K \; q^2 n_\perp{}^2(q) V \,. \tag{2.25}$$

where *V* is the volume. Using equipartition theorem i.e. equating the energy of each mode with the thermal energy $\frac{1}{2} k_B T$, we get

$$\left\langle |n_\perp(q)|^2 \right\rangle = \frac{k_B T}{V K q^2} \,. \tag{2.26}$$

If $q \to 0$, the fluctuation amplitude $\left\langle |n_\perp(q)|^2 \right\rangle$ is large. Let us assume that a stabilizing electric field is applied along the *z* direction. Therefore the energy density is given by the sum of the $n_\perp$ - dependent part of the field energy plus the distortion energy

$$F = F_d + F_e = \frac{1}{2} K (\nabla n_\perp)^2 + \frac{\Delta\varepsilon}{8\pi} n_\perp^2 E^2 \tag{2.27}$$

where *E* is the applied electric field and $\Delta\varepsilon$ (> 0) is the dielectric anisotropy. Using the equipartition theorem the fluctuation amplitude can be expressed as

$$\left\langle |n_\perp(q)|^2 \right\rangle_E = \frac{k_B T}{V} \frac{1}{K\ q^2 + \dfrac{\Delta\varepsilon\ E^2}{4\pi}} = \frac{k_B T}{V} \frac{1}{K\ \left(q^2 + \xi^{-2}\right)} \tag{2.28}$$

where $\xi(E) = \left(\dfrac{K}{\Delta\varepsilon / 4\pi} \right)^{1/2} \dfrac{1}{|E|}$ is called the electric coherence length. It is seen from equation (2.28) that due to the electric field the fluctuation amplitude is reduced. The inverse Fourier transform of equation (2.28) gives

$$\left\langle n_\perp^2 \right\rangle_E \approx \frac{k_B T}{2\pi^2 K} \left(q_c - \frac{\pi}{2\xi} \right) \tag{2.29}$$

where q_c is the cut off wave vector, given by $2\pi / a$, where *a* is of the order of a molecular dimension. Using $\left\langle n_z^2 \right\rangle = 1 - \left\langle n_x^2 \right\rangle - \left\langle n_y^2 \right\rangle = 1 - 2\left\langle n_\perp^2 \right\rangle$ and $S = \left(\dfrac{3}{2} \left\langle n_z^2 \right\rangle - \dfrac{1}{2} \right)$, the enhancement of order parameter due to the quenching of the director fluctuations by electric field is given by [4]

$$\delta S = \frac{3}{2} \left[\left\langle n_z^2 \right\rangle_E - \left\langle n_z^2 \right\rangle_0 \right] = 3 \left[\left\langle n_\perp^2 \right\rangle_0 - \left\langle n_\perp^2 \right\rangle_E \right] \tag{2.30}$$

$$\delta S = \frac{3 k_B T}{4\pi\ K^{3/2}} \left(\frac{\Delta\varepsilon}{4\pi} \right)^{1/2} |E| \ . \tag{2.31}$$

It is noticed that the enhancement in the order parameter due to the electric field is <u>linearly</u> proportional to the modulus of the applied electric field. This is in addition to the quadratic dependence of δS on field arising from the Kerr effect (see equation (2.19)). Similarly δS can be calculated due to the magnetic field. Some early experiments in late 70s [12] using a magnetic field showed that $\Delta n_H - \Delta n_0 \propto H$.

Durand et al performed high electric field experiments on 5CB[4]. They measured the order parameter as a function of electric field at various temperatures (Fig.(2.5)) and analysed the enhancement of *S* with field in terms of both the linear and quadratic effects. We have obtained the shift in the paranematic–nematic transition temperature (T_{PN}) from the data of Fig.(2.5). It is plotted as a function of field in Fig.(2.6). It may be pointed out that the shift is linearly proportional to the electric field unlike the prediction of the Landau de Gennes theory, which gives a quadratic dependence (see equation (2.22)).

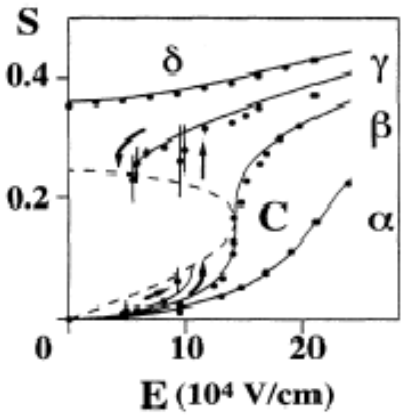

Figure 2.5: Variation of order parameter *S*(*E*) as a function of electric field ($E \parallel \hat{n}$) in the nematic liquid crystal 5CB at various temperatures near the critical point *C*. α : T=T_{NI}+1.55*K*; β : T_c=T_{NI}+0.65*K*; γ : T=T_{NI}+0.25*K*; and δ : T=T_{NI}-0.15*K*. The solid lines are fit to the experimental data using the Landau-de Gennes model. The dashed line is the spinodal. (adapted from ref.[4])

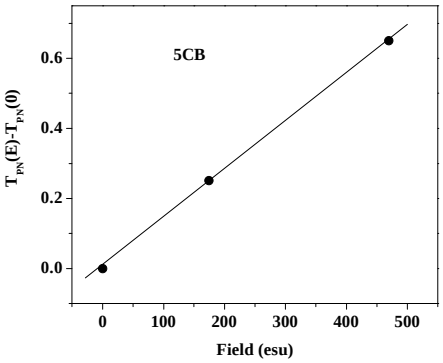

Figure 2.6: Variation of the shift in the paranematic–nematic transition temperature ($\Delta T_{PN} = T_{PN}(E) - T_{PN}(0)$) as a function of applied field. Data points (filled circles) are derived from Fig.(2.5)

It was reported by Geetha et al [5] that the shift in the nematic-smectic transition temperature (T_{AN}) is proportional to E^2 and is consistent with the prediction of Landau theory. The variation of T_{AN} is shown in Fig.(2.7) as a function of electric field. In this case the elastic constant K_3 diverges as the N-SmA transition is approached and the director fluctuations are quenched in the SmA phase. Therefore only the Kerr effect contribution from dielectric anisotropy is important. On the other hand, the linear variation of T_{PN} as a function of field indicates that the quenching of director fluctuations are very important near the paranematic –nematic phase transition. The earlier workers did not emphasise this aspect.

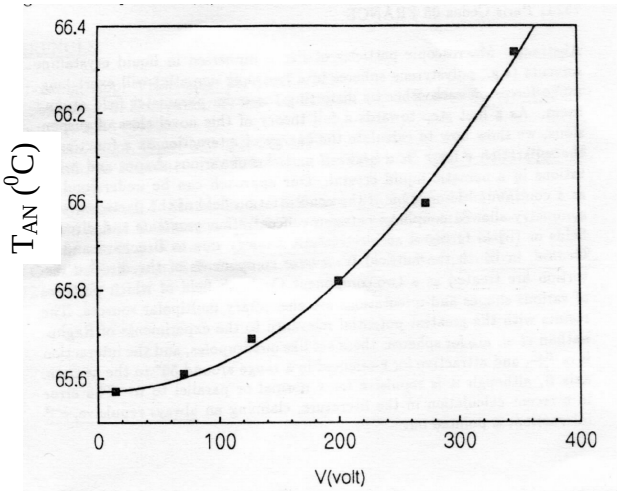

Figure 2.7: T_{AN} as a function of applied electric field in 8OCB. The symbols are experimental data. The calculated variation (continuous line) corresponds to the prediction of the Landau theory that the shift in transition temperature is proportional to E^2.(adapted from ref.[5])

2.2.5 Nematic–Paranematic Phase Transition under an External Electric Field for a System with $\Delta\varepsilon < 0$

Studies on the effect of strong electric fields on liquid crystals with negative dielectric anisotropy $(\Delta\varepsilon < 0)$ are interesting because the phase diagram is very different in nature compared to that in a system with $\Delta\varepsilon > 0$ [13]. In the former system a strong

dipolar group makes a large angle with the long axis of the molecule. To study the electric field effect, a nematic liquid crystal with $\Delta\varepsilon < 0$ is sandwiched between two ITO (indium-tin oxide) coated glass plates, which are treated for planar alignment and the field is applied between the plates (along the z -axis) as shown in Fig.(2.8). In the paranematic phase the dipoles of the molecules tend to align along the field direction. As a result the long molecular axes tend to be perpendicular to the field direction. It should be pointed out that in the paranematic phase the distribution of azimuthal angles of the molecules in the (XY) plane perpendicular to the field is random. The projections of the long axes of the molecules in the XY plane are shown in Fig.(2.8).

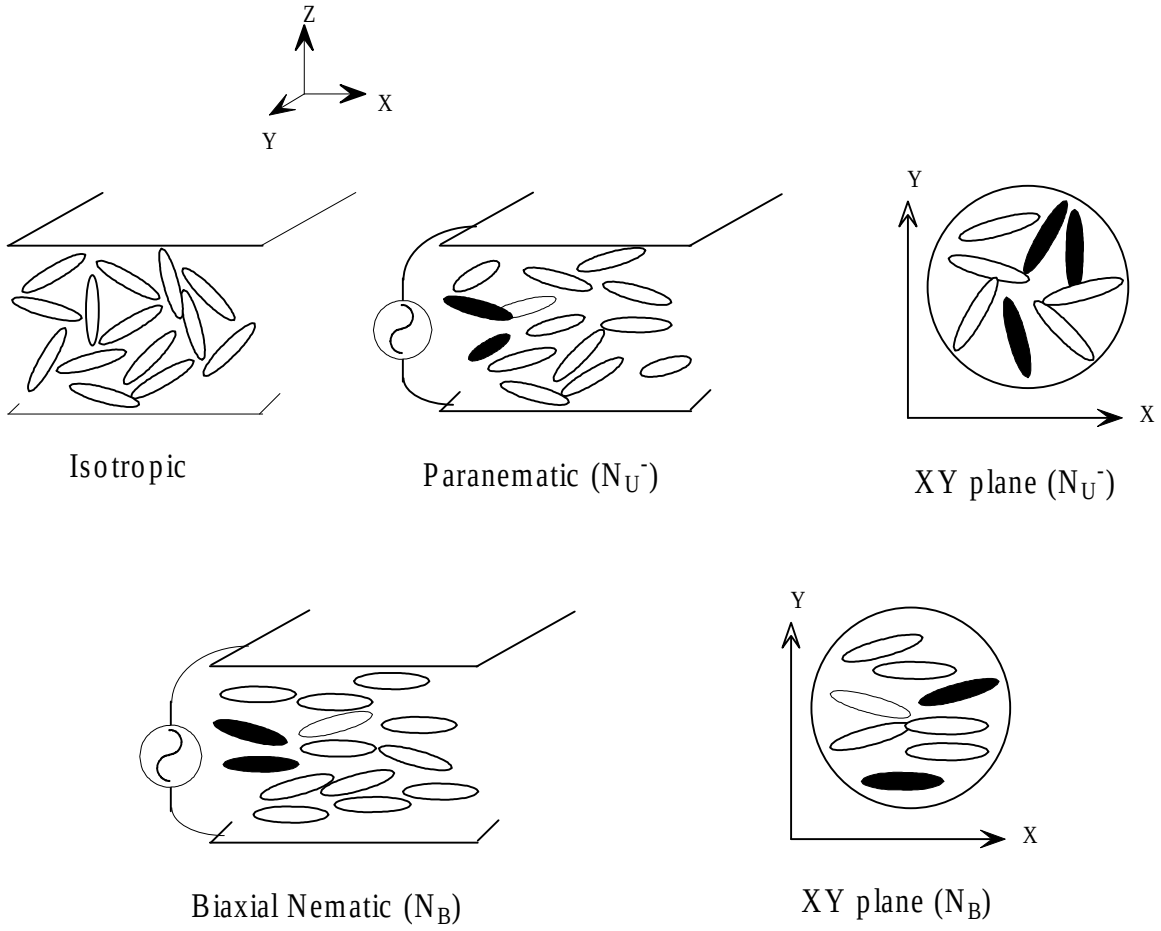

Figure 2.8: Schematic representation of the field induced paranematic (N_U^-) and biaxial nematic (N_B) liquid crystals. The relative size of the molecules is exaggerated for clarity.

In the paranematic phase the distribution function of the long axes around the field direction shows a small peak at $\pi/2$. With increasing field the peak height increases in the paranematic phase as shown schematically in Fig.(2.9). Therefore the order parameter (S) in the paranematic phase becomes *negative* giving rise to negative uniaxial (N_U^-) phase as depicted schematically in Fig.(2.8).

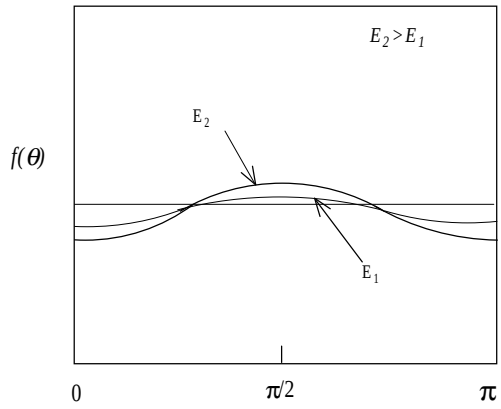

Figure 2.9: Schematic representation of the distribution function in the presence of electric field ($\Delta\varepsilon < 0$) above T_{PN}. Dotted line represents the distribution function without field in the isotropic phase, and the continuous line represents the same with field in the paranematic phase. The peak around $\pi/2$ is exaggerated for clarity.

When the system is cooled under the field below the paranematic–nematic transition temperature the long axes of the molecules tend to align in a preferred direction (x-axis) because of the surface interaction with the treated plates. In the nematic phase there is a partial quenching of the director fluctuations due to electric fields in the ZX plane (Fig.(2.8)), thus the fluctuations in the ZX plane are different from those in the XY plane perpendicular to the field. Therefore the differential quenching of fluctuations leads to an induced biaxiality under field [14-15]. Under the field the paranematic to nematic transition corresponds to uniaxial nematic (N_U^-) to biaxial nematic (N_B) transition. With increasing field N_U^- to N_B transition temperature is shifted to higher values and the order parameter is increased in the N_B phase. The jump in the order parameter reduces and

finally the transition becomes continuous above the tricritical field, at which the first order transition goes over to a second order phase transition as shown in Fig.(2.10). In Table-I the field effect on the different phases is summarised.

Table-I

The effect of an electric field on the isotropic- nematic phase transition

Phase in zero field	Phase in nonzero field	
	$\Delta\varepsilon > 0$	$\Delta\varepsilon < 0$
I	N_U+	N_U-
N_U+	N_U+	N_B

Thus the application of an external electric field to a nematic liquid crystal with negative dielectric anisotropy induces biaxial ordering. We use the tensor order parameter $Q_{\alpha\beta}$ to be able to describe this. Considering up to the fourth order term in the expansion, the Landau-de Gennes free energy density in the presence of an external electrical field can be written as [10]

$$F = -\frac{1}{8\pi}\Delta\varepsilon_0 E_\alpha E_\beta Q_{\alpha\beta} + \frac{1}{2}ATrQ^2 + \frac{1}{3}BTrQ^3 + \frac{1}{4}C\left(TrQ^2\right)^2 \qquad (2.32)$$

where A (= a (T-T^*)), B, C are Landau coefficients which will be numerically different from those in equation (2.19). The tensor order parameter $Q_{\alpha\beta}$ is defined as

$$Q_{\alpha\beta} = \begin{pmatrix} -\frac{1}{2}(x+y) & 0 & 0 \\ 0 & -\frac{1}{2}(x-y) & \\ 0 & 0 & x \end{pmatrix} \qquad (2.33)$$

where x is analogous to S defined earlier ($x = \frac{2}{3}S$) and y is the biaxial order parameter which distinguishes between two directions orthogonal to the director. Using equation (2.33) we find

$$TrQ_{\alpha\beta}^{2} = \left(\frac{3x^{2} + y^{2}}{2} \right) \tag{2.34a}$$

$$TrQ_{\alpha\beta}^{3} = \frac{3}{4}\left(x^{3} - xp^{2}\right). \tag{2.34b}$$

Using equations (2.32), (2.34a) and (2.34b) the free energy density can be written in terms of order parameters *x*, *y* as

$$F(x, y) = \alpha(x) + y^{2}\beta(x) + y^{4}\gamma \tag{2.35}$$

with $\alpha(x) = -hx + \frac{3}{4}Ax^{2} + \frac{1}{4}Bx^{3} + \frac{9}{16}Cx^{4}$,

$$\beta(x) = \frac{1}{4}A - \frac{1}{4}Bx + \frac{3}{8}Cx^{2}, \qquad \text{and} \qquad \gamma = \frac{1}{16}C.$$

where $h = \frac{1}{8\pi}\Delta\varepsilon_{0}E_{\alpha}E_{\beta}$. Minimising $F(x, y)$ with respect to *y*, we get

$$y = 0 \text{ (uniaxial)}, \tag{2.36a}$$

$$y^{2} = -\beta(x)/2\gamma \text{ (biaxial)}, \tag{2.36b}$$

The solution (2.36b), which depends on *x*, and hence on *h* is real when $\beta(x) < 0$ as $\gamma > 0$. The free energies in the two phases are obtained by using equations (2.35), (2.36a) and (2.36b) as

$$F_{U}(x) = \alpha(x) \text{ when } \beta(x) \geq 0 \qquad \text{(uniaxial)}, \tag{2.37a}$$

$$F_{B}(x) = \alpha(x) - \beta^{2}(x)/4\gamma. \qquad \text{(biaxial)} \tag{2.37b}$$

Whenever the biaxial solution is allowed, $F_{B}(x) < F_{U}(x)$. The equilibrium order parameters in the N_B phase could be found by minimising the free energy density F_B, and are given by [10]

$$x = \frac{B}{12C}\left[1 + (1 - \eta + \zeta)^{1/2}\right], \tag{2.38a}$$

$$y = \frac{B}{2\sqrt{2}C}\left[1 - \frac{5}{2}\eta - \frac{1}{6}\zeta + (1 - \eta + \zeta)^{1/2}\right]^{1/2}, \tag{2.38b}$$

with $\eta = 6AC/B^{2}$, $\zeta = 12C^{2}h/B^{3}$. For a second order uniaxial-biaxial phase transition at $x=x_0$, the following conditions are satisfied [10]:

$$\beta(x_0) = 0, \tag{2.39a}$$

$$\alpha''(x_0) = 0, \tag{2.39b}$$

$$\left(\frac{d^2 F_B(x)}{dx^2}\right)_{x=x_0} \geq 0\,. \tag{2.39c}$$

Using these conditions uniaxial to biaxial transition is found to be first order for $|h| < |h_{TCP}|$ and second order for $|h| > |h_{TCP}|$. The point $|h| = |h_{TCP}|$ is a tricritical point. The location of the tricritical point is given by equations (2.39a), (2.39b) with (2.39c) holding as an equality,[10]:

$$|h_{TCP}| = \frac{1}{64}\frac{B^3}{C^2}\,. \tag{2.40a}$$

The temperature and the orientational order parameter at the tricritical point are given by

$$T_{TCP} = T_{NI}^0 + \frac{31B^2}{864aC} \tag{2.40b}$$

$$S_{TCP} = \frac{1}{12}\frac{B}{C}\,. \tag{2.40c}$$

The calculated phase diagram using this model for nematic liquid crystals with negative dielectric anisotropy as a function of reduced temperature is shown in Fig.(2.10).

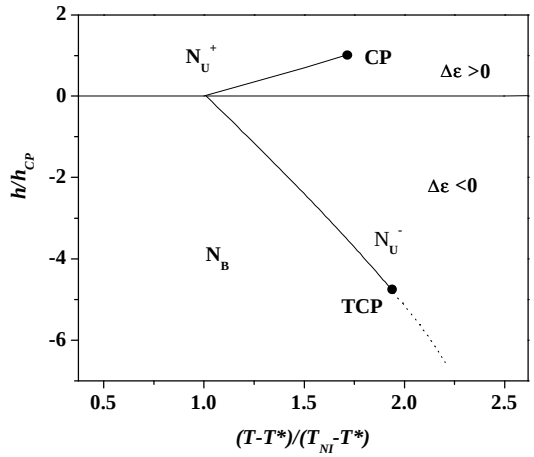

Figure 2.10: Composite *h, T* phase diagram of nematics with both $\Delta\varepsilon > 0$ and $\Delta\varepsilon < 0$. Thick lines indicate first order transitions, dashed line the second order transition: CP and TCP are critical and trictrical points. (adapted from ref.[10])

The field-induced biaxiality in the system with $\Delta\varepsilon < 0$ arises due to the quenching of the director fluctuations as well as the Kerr effect. The only electric field experiment on system with $\Delta\varepsilon < 0$ was reported by Dunmur et al [14-15]. They found that the induced biaxiality is linearly proportional to the modulus of the applied electric field, which originates mainly from the quenching of director fluctuations. Using a sensitive optical modulation technique they measured the field induced biaxial order parameter in the nematic phase which is very small, ~10^{-3} at ~100 esu.

In this chapter we report the first experiment on the effect of strong electric field (~550 esu) on the paranematic-nematic transition on a system with large negative dielectric anisotropy.

The main difficulty in conducting high electric field experiments on liquid crystals is the heating of the sample due to ionic conductivity as well as dielectric relaxation. There can also be hydrodynamic instability [11] for the systems with $\Delta\varepsilon < 0$. To minimise the heating effect Durand et al [3] applied an electric field of short pulse duration (~10 to 100 μs) with long *off* period giving a small duty cycle. In this technique it takes a long time (~ 40 minutes) to collect each data point. They measured birefringence of the sample under the field and calculated the order parameter for materials with $\Delta\varepsilon > 0$.

We have adapted the technique developed by Geetha et al [5]. In this technique, the local temperature of the sample is measured under the field and the data points are collected continuously. This technique enables us to perform optical as well as electrical measurements simultaneously on materials with negative $\Delta\varepsilon$.

In this chapter we report the following results on a material with $\Delta\varepsilon < 0$: (a) electric field induced enhancement of birefringence (b) shift in the uniaxial to biaxial nematic transition temperature (T_{PN}) with field (c) evidence for surface transition (d) divergence of order parameter susceptibility near the second order uniaxial to biaxial nematic transition temperature as measured by third harmonic electrical signal (e) detection of a small second harmonic electrical signal near uniaxial to biaxial nematic transition under a strong field.

2.3 Experimental

The block diagram of the experimental setup is shown in Fig.(2.11). In order to measure local temperature of the sample we use an evaporated nickel (Ni) film to design a temperature sensor. Ni shows a high temperature coefficient of resistance (~6200 ppm/K). A thin film (~0.2μm) of nickel is vacuum coated on a plane glass plate. A zigzag pattern of nickel film which has a strip width of 200μm and total length of 5cm is etched photolithographically. The resistance of the pattern is ~100 to 200Ω. The Ni thermometer is calibrated in each cell to measure the local temperature. The thermometer is covered with a thin insulating layer of SiO on which a circular aluminum electrode (with 0.5cm diameter) is vacuum evaporated. In order to reduce the field gradient at the edges a guard ring is designed just outside the Al electrode with a separation of 100μm as

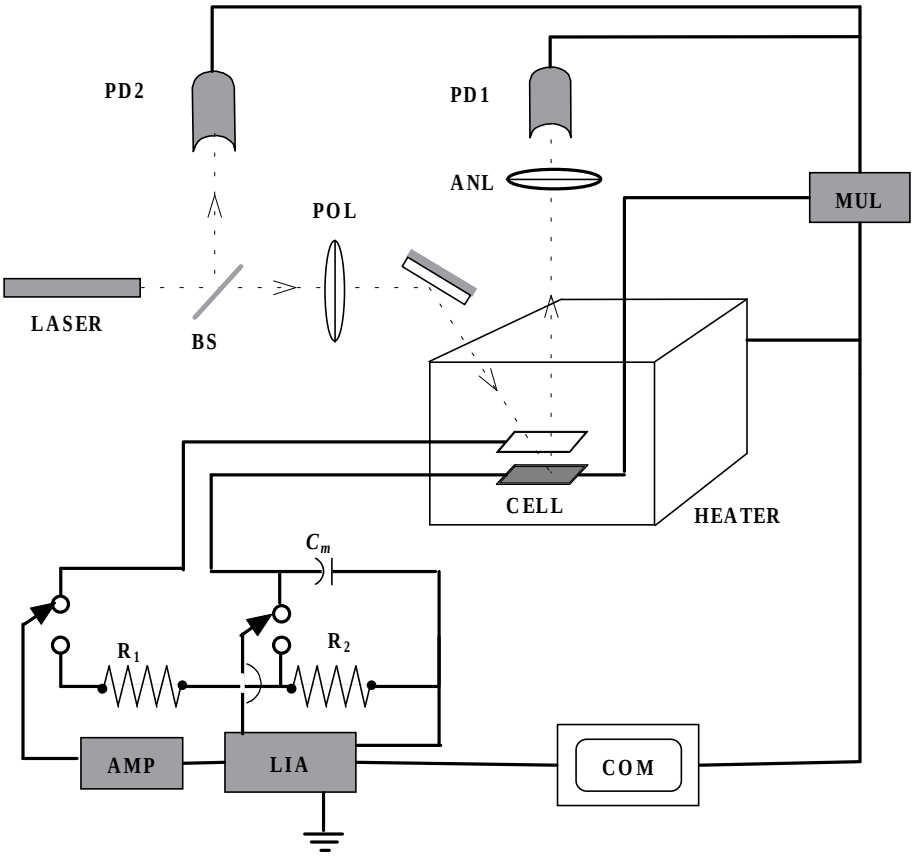

Figure 2.11: Schematic diagram of the experimental setup. Photodiodes (PD1, PD2). Polariser (POL), Analyser (ANL), Multimeter (MUL), Voltage Amplifier (AMP) Lock in amplifier (LIA), Resistances (R_1, R_2), Computer (COM). The reflection angle of the laser beam is exaggerated for clarity.

shown in Fig.(2.12). The top electrode is an ITO coated glass plate. SiO is coated on both the plates at a grazing angle of 30^0 using vacuum evaporation. On such a plate, the director is aligned orthogonal to the incident direction of SiO beam. Mylar spacers are used to obtain the required cell thickness. The sample thickness is measured outside the electrode area by an interferometric technique described in chapter-I.

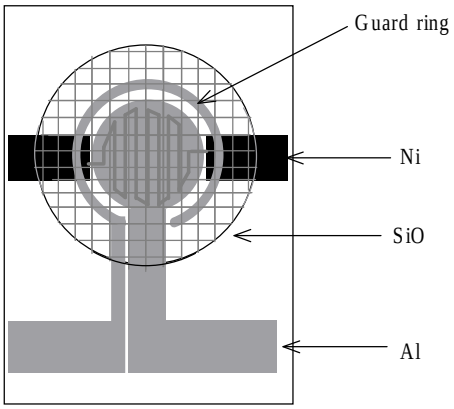

Figure 2.12: Schematic diagram of the lower electrode. There is an insulating SiO coating between Ni thermometer and the Al electrode. Notice the zigzag pattern of the Ni thermometer.

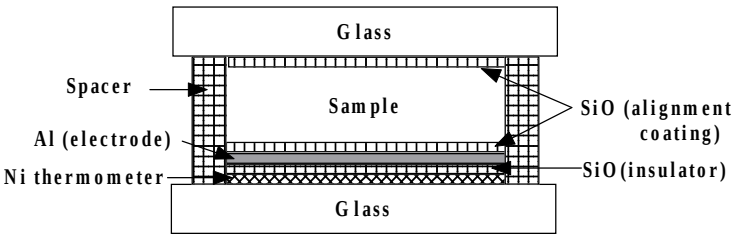

Figure 2.13: Schematic of the side view of the cell (not to scale).

Typical cell thickness used for the experiments is ~16μm. The electrical connections to the two plates are made through copper wires which are soldered using an ultrasonic soldering gun. The cross section of a typical cell is schematically shown in Fig.(2.13). The cell is mounted in a hot stage (INSTEC HS1) which itself is placed on the rotating stage of the microscope (model ORTHOPLAN). The temperature is controlled to

an accuracy of 0.008^0C. The cell is filled with the sample in the isotropic phase and on slow cooling to the nematic range, a well-aligned sample is obtained.

The output voltage of a lock-in amplifier (LIA, model SRS 830) is connected to a high gain voltage amplifier (TREK, model 601-2). The output of the amplifier is connected to one of the two branches shown in Fig.(2.11). In one branch there is a potential divider circuit, which is made of two resistors (R_1=1MΩ and R_2=100Ω) connected in series. The potential divider circuit is used to measure the phase and amplitude of the amplified voltage. In another branch the sample cell is connected in series with a capacitor C_m (~ $1\mu F$). A manual DPDT switch is used to switch between the two branches. The phase and amplitude of the current flowing in the cell are measured across the capacitor C_m. The LIA can be used to measure higher harmonic signals also. Two zenor diodes with their opposite polarities interconnected as shown in Fig.(2.14) was connected across the input of the LIA to protect it from accidental high currents, (for *eg* if the cell shorted). Using impedance analysis, we measure the capacitance (C_S) and resistance (R_S) of the sample.

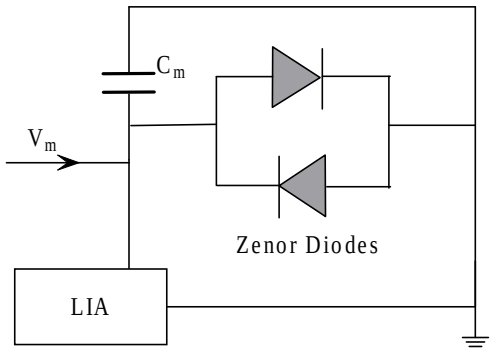

Figure 2.14: A block diagram of the zenor diodes circuit to protect the lock-in amplifier from large currents.

If V_0 and ϕ_0 are the amplitude and phase at the output of the amplifier and V_m and φ_m are the same measured across the capacitor C_m, it can be shown (see section 4.3 of chapter-IV) that the capacitance and resistance of the sample are given by

$$R_S = \frac{Y}{\omega \sin\alpha}, \qquad (2.41)$$

$$C_S = \frac{X}{Y}, \tag{2.42}$$

where $X = \cos\alpha - Q$, $Y = \frac{\sin^2\alpha + X^2}{C_m Q}$, $Q = \frac{V_m}{V_0}$, $\alpha = \phi_0 - \phi_m$, and $\omega = 2\pi f$, f being the frequency of the applied signal. The dielectric constant is given by the ratio C_S / C_0, where C_0 is the capacitance of the empty cell. Using a set of standard capacitors and resistors in parallel connected in place of the cell, the measuring system is calibrated. It is found that the stray capacitance is ~ 2 *pF*. The accuracy of the measured capacitance is ~1% and that of the resistance is ~ 5 %.

The lower electrode is opaque due to the Al and Ni coatings, and it is not possible to perform optical measurements in the transmission mode. We have used an ITO coated glass plate as the top electrode which enables us to perform optical measurements in the reflection mode of the microscope. A laser (He-Ne, λ= 632.8*nm*) beam is passed through a polariser (POL) and made to be incident on the sample. The Al electrode reflects the laser beam. The reflected beam is passed through an analyser (ANL), which is crossed with respect to the polariser. A photodiode (PD1, model Centronics OSD-5) is used to measure the reflected intensity. The stability of the laser intensity is monitored by another photodiode (PD2). A multimeter (MUL, Keithley model 2000) measures the output voltages of both the photodiodes as well as the Ni resistance.

The temperature variation of the optical intensity is measured in the homogeneously aligned sample. Transmitted intensity through a uniformly aligned sample is given by

$$I_t = \frac{\sin^2 2\zeta}{2}\left(1 - \cos\Delta\varphi\right), \tag{2.43}$$

where ζ is the angle made by the polariser with the optic axis and the phase difference

$$\Delta\varphi = \frac{2\pi}{\lambda}\Delta n\left(2d\right) \tag{2.44}$$

$\Delta n = n_e - n_o$, where n_e and n_o are the extraordinary and ordinary refractive indices of the liquid crystal medium. Here *d* is the sample thickness and the factor 2 comes because the light travels across the sample thickness twice in the reflection mode. The angle ζ is set at 45^0 to optimise the measurements. The birefringence is calculated from the measured

intensity. The typical frequency and voltage ranges used in the experiments are 1111-15111 Hz and 5 to 270 V respectively. The sample 4′-butyl-4 heptyl-bicyclohexyl-4-carbonitrile (CCN-47) was obtained from Merck and used in the experiment without further purification. The chemical structure of the molecule is shown in Fig.(2.15). It has the following phase transitions: Cr 28 SmA 30.6 N 59.7 I. This compound exhibits a large negative dielectric anisotropy ($\Delta\varepsilon$ = -8.0 at 20 ^{0}C) and the smectic phase can be supercooled to room temperature. The measurements are completely controlled by a computer, using a suitable program. All the experiments are performed while cooling the sample from the paranematic phase.

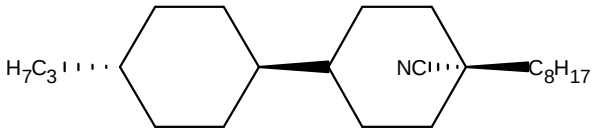

Cr 28 SmA 30.6 N 59.7 I

Figure 2.15: Chemical structure and the phase sequence of the compound used in the experiments. Temperatures are given in degree Celsius.

2.3.1 Results and Discussion

A typical variation of Ni resistance with the temperature is shown in Fig.(2.16).

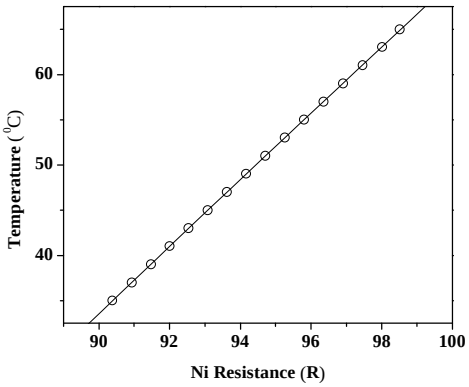

Figure 2.16: Temperature calibration curve for the nickel resistance thermometer. Open circles are the experimental data and the line is a polynomial ($T = a+bR+cR^2$) fit to the data.

The birefringence (Δn) is calculated from the transmitted intensity using equations (2.43) and (2.44). The variation of Δn over a wide temperature range (~20 ^{0}C) in the nematic phase is shown in Fig.(2.17). It is noticed that Δn is very small ~0.016 at 0.5 ^{0}C below T_{NI} and increases to 0.031 at 20 ^{0}C below T_{NI} in view of the saturated rings of the molecules. The birefringence Δn_0 of a completely ordered sample is determined from the temperature dependence of Δn, which can be approximated well for nematic liquid crystals by [16]

$$\Delta n = \Delta n_0 \left(1 - \frac{T}{T_1}\right)^{\beta} \tag{2.45}$$

where T_1 and β are adjustable parameters. A least squares fit to the experimental data with equation (2.45) is shown in Fig.(2.17). The value of the fitted parameters are T_1 = 333.0K, which is 0.3 ^{0}C higher than $T_{NI,}$ Δn_0 = 0.0576 and β = 0.23. The value of β is typical for nematic liquid crystals [11].

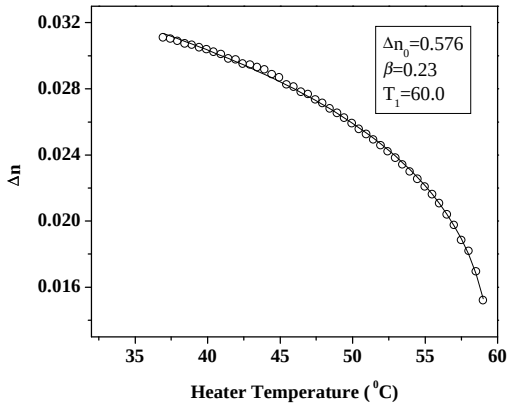

Figure 2.17: Variation of Δn as a function of temperature. Circles are the experimental data and the continuous line is a theoretical fit to the to equation (2.45). Cell thickness: 16.8μm.

We have measured $\varepsilon_{\perp}$ in a homogeneously aligned sample and $\varepsilon_{\parallel}$ in a homeotropically aligned sample. The cell thicknesses used for the experiment are 8.5μm and 7μm respectively in the two cases. Both the measurements are made at applied voltage of 0.2 V and a frequency of 4111 Hz. The applied voltage (0.2V) is much lower

than the threshold voltage for Freedericksz transition in the homeotropic cell. The variations of dielectric constants $\varepsilon_{\parallel}$ and $\varepsilon_{\perp}$ are shown as functions of the heater temperature in Fig.(2.18). It is noticed that $\varepsilon_{\perp}$ is larger than $\varepsilon_{\parallel}$ in the nematic as well as in the smectic phases, the N-SmA transition occurring at 30.6 ^{0}C. The variation of $\varepsilon_{\parallel}$ across the N-SmA transition temperature is smooth whereas a small increase is observed in $\varepsilon_{\perp}$. The dielectric anisotropy $\Delta\varepsilon = (\varepsilon_{\parallel} - \varepsilon_{\perp})$ at the NI transition is ≈ -3 and increases to ≈ -6 at 30 ^{0}C below T_{NI}. The mean dielectric constant $\bar{\varepsilon}$ is calculated using the formula $\bar{\varepsilon} = (\varepsilon_{\parallel} + 2\varepsilon_{\perp})/3$. At T_{NI}, $\bar{\varepsilon} = \varepsilon_{is} \approx 7.2$ and as the temperature is lowered down to the N-SmA transition $\bar{\varepsilon}$ is increased to ≈ 8. The increase in $\bar{\varepsilon}$ is ~4 % at T_{NI} -15^0 (N phase) and ~10 % at T_{NI} -30^0 (in the SmA phase).

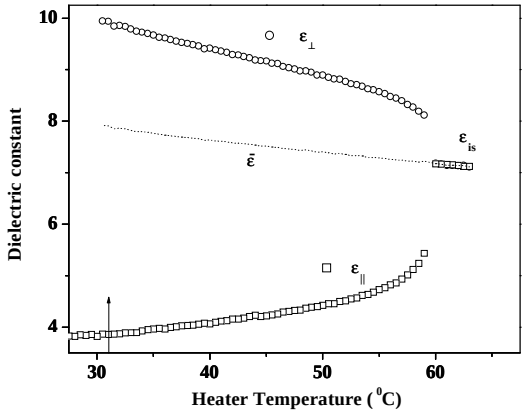

Figure 2.18: Variations of $\varepsilon_{\parallel}$ and $\varepsilon_{\perp}$ as functions of heater temperature. Applied voltage: 0.2 V and frequency: 4111 Hz. ε_{is} is the dielectric constant in the isotropic phase. The mean value in the nematic phase is $\bar{\varepsilon} = (\varepsilon_{\parallel} + 2\varepsilon_{\perp})/3$, which is shown by a dotted line. The vertical arrow denotes N-SmA transition temperature.

According to the Maier and Meier theory (see equation (1.13) in chapter-I)

$$\bar{\varepsilon} = 1 + 4\pi \frac{N_A \rho\ hF}{M}\left(\bar{\alpha} + \frac{F\mu^2}{3k_B T}\right). \qquad (2.46)$$

The second term in the bracket is due to the contribution of the orientational polarisation of the dipole moments. In the nematic phase $\bar{\varepsilon}$ can increase with decreasing temperature

due to the increase in the density (ρ) and the contribution from orientation polarisation. Experimentally it is reported in a nonpolar compound that $\bar{\varepsilon}$ increases by ~2 % at 15^0 below NI transition temperature due to increase in density alone [17]. The excess variation in the highly polar compound used by us is due to the contribution of the orientation polarisation, which increases with decreasing temperature as seen in equation (2.46).

We have also measured the threshold voltage for Freedericksz transition at several temperatures. The measurement is made at a frequency 4111 Hz. The experimental procedure is described in chapter-I. Since the dielectric anisotropy of the compound is negative the experiment is performed in a homeotropically aligned sample. In this case the threshold voltage is given by $V_{th} = \pi\sqrt{K_3 / \varepsilon_0 \Delta\varepsilon}$ where K_3 is the bend elastic constant and ε_0 is the dielectric constant of the free space. Using V_{th} and $\Delta\varepsilon$ we calculate K_3 at several temperatures. The variation of K_3 as a function of heater temperature is shown in Fig.(2.19). It is noted that K_3 is ~0.2×10^{-6} dynes at a temperature of 1 ^{0}C below T_{NI} and it follows an S^2-dependence near T_{NI}, where S is the order parameter. As the nematic to smectic transition (30.6 ^{0}C) is approached, K_3 is expected to diverge and the curvature of the variation changes sign around 40 ^{0}C. We could not measure V_{th} below 32 ^{0}C due to the occurrence of hydrodynamic instabilities (EHD) in the sample under the electric field

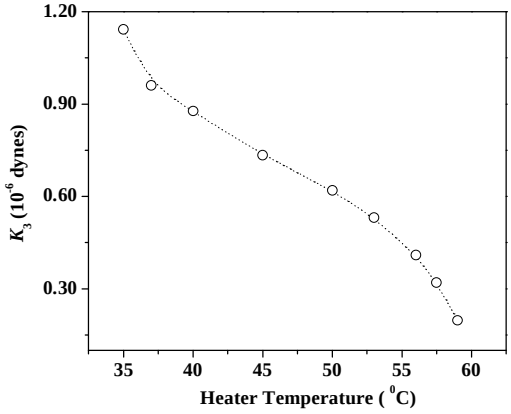

Figure 2.19: Variation of the bend elastic constant K_3 as a function of temperature. Points are experimental data and the dotted line is drawn as a guide to the eye.

at these temperatures. Surprisingly we did not find any EHD in the nematic phase of this compound until we reach T_{AN} . The only other experimental investigation on this compound was by Lavrentovich et al [18] who studied the growth pattern under electric fields in the SmA phase in the homeotropic geometry.

The variation of Δn as functions of local temperature across the paranematic to nematic transition at different fields are shown in Fig.(2.20). These data are collected in temperature steps of 0.5 ^{0}C. It is observed that the individual curves at different fields are clearly seen down to ~2 ^{0}C below the transition point. Our main interest is to study the effect of strong fields on the paranematic-nematic transition. Therefore we have conducted detailed measurements across the transition over a 0.5^0 temperature range with temperature steps of 0.01 ^{0}C.

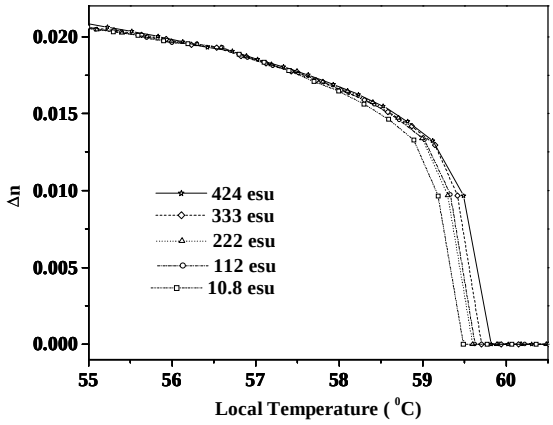

Figure 2.20: Variations of birefringence in the paranematic and nematic phases as functions of local temperature at different fields. Points are experimental data and the continuous lines are drawn as guides to the eye. Cell thickness: 16.8μm. Frequency of the applied field: 15111 Hz (1esu = 300V/cm).

Variations of Δn as well as $\varepsilon_\perp$ are shown as functions of local temperature at various fields in Fig.(2.21) and Fig.(2.22) respectively. The data shown in these two figures are collected after several thermal cycles of the sample. The local temperature is the temperature measured by the Ni resistance thermometer. The following important features are noted from Fig.(2.21): (i) with increasing field (a) Δn is enhanced in the

nematic phase and (b) the paranematic to nematic (N_U^- -N_B) transition temperature (T_{PN}) is shifted toward higher values (ii) Δn sharply rises from the zero value as the temperature is lowered in the phase transition region (iii) separations among the curves are quite wide close to the transition point and are reduced as the temperature is lowered in the nematic phase.

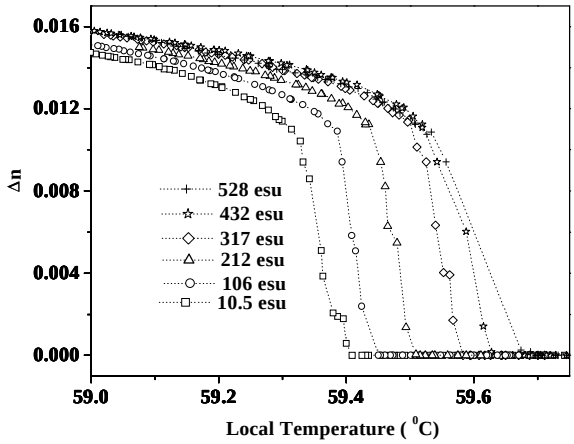

Figure 2.21: Variation of birefringence across the paranematic-nematic transition region as a function of local temperature at different fields. Cell thickness: 16.8μm. Frequency of the applied field: 4111 Hz. Points are the experimental data and the dotted lines are drawn as guides to the eye.

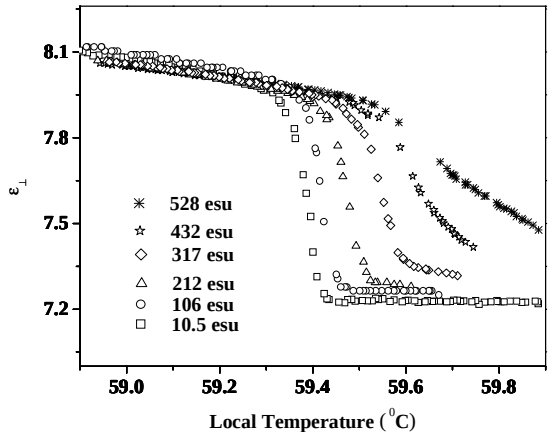

Figure 2.22: Variation of dielectric constant across the paranematic-nematic transition region as a function of local temperature at different fields. This data and the data shown in Fig.(2.21) were obtained simultaneously.

An independent experiment was performed on a fresh sample. The overall response is similar to that of the first sample except that the field free transition temperature is slightly higher in the fresh sample. Variations of Δn as well as $\varepsilon_{\perp}$ on this sample are shown as functions of local temperature at various fields in Fig.(2.23) and Fig.(2.24) respectively.

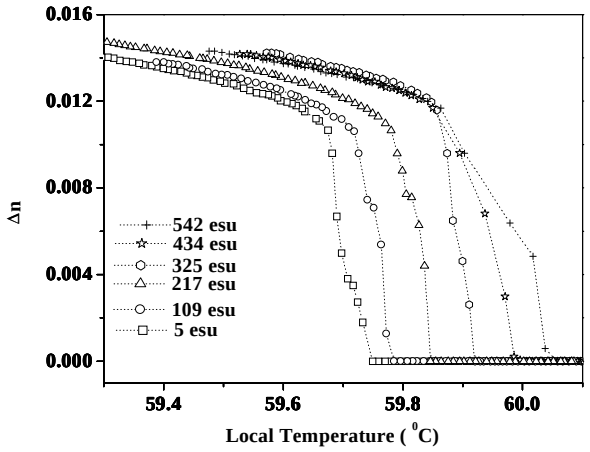

Figure 2.23: Variation of birefringence across the paranematic-nematic transition region as a function of local temperature at different fields on a fresh sample. Cell thickness: 16.4μm. Frequency of the applied field: 4111 Hz.

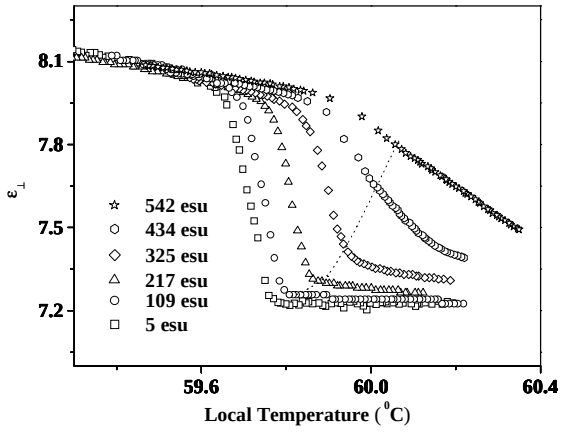

Figure 2.24: Variation of dielectric constant across the paranematic-nematic transition region as a function of local temperature at different fields. These data and the data shown in Fig.(2.23) were obtained simultaneously. Dotted line connects the temperatures at which Δn starts to rise from zero value.

In order to see the influence of frequency of the applied field we made another independent optical measurement on a fresh sample at a frequency of 15111 Hz. Variations of Δn up to 334 esu are shown in Fig.(2.25) as a function of local temperature. It is noticed that the overall response is similar to that of the second sample.

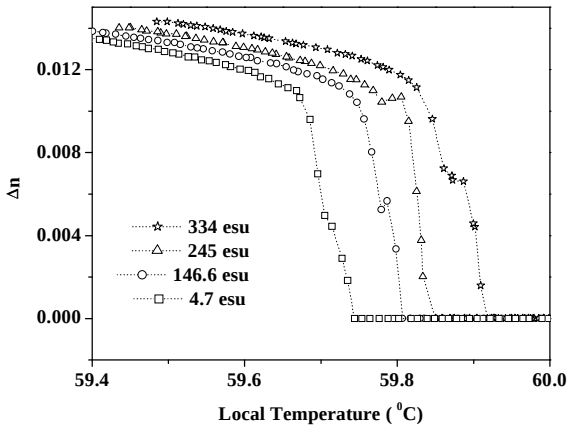

Figure 2.25: Variation of Δn across the paranematic-nematic transition region as a function of local temperature at different fields. Cell thickness: 16.4μm. Frequency of the applied field: 15111 Hz.

The temperature at which Δn starts rising from zero value is a measure of the paranematic to nematic transition temperature (T_{PN}) (However, see later discussion). The variations of T_{PN} obtained from Fig.(2.21) and Fig.(2.23) are shown as functions of field in Fig.(2.26). A large shift in T_{PN} (~0.3^0) is measured between 5 to 550 esu. The important result is that T_{PN} varies linearly with the r.m.s field. In the fresh sample T_{PN} is about 0.4 ^{0}C higher than in the recycled one. However the slopes of the two curves shown in Fig.(2.26) are the same. It may be mentioned that a quadratic variation of T_{PN} is predicted by the Landau de Gennes theory (only an E^2 term occurs in the free energy). The linear variation of T_{PN} as a function of field indicates that the quenching of director fluctuations not only increases the order parameter but it also has a strong influence on the phase transition. This point was not recognised in earlier high electric field experiment on systems with $\Delta\varepsilon > 0$ [3]. In our experiment we precisely measure the local

temperature of the sample under field by a nickel resistance thermometer. It enables us to measure the transition temperature at various fields accurately.

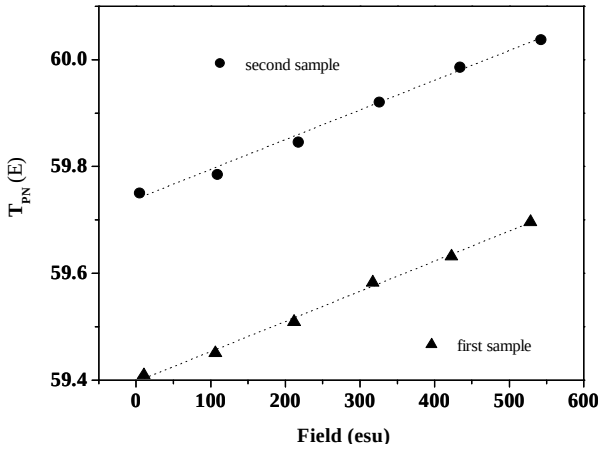

Figure 2.26: Variation of paranematic-nematic transition temperature (T_{PN}) as a function of applied field. Data corresponding to the filled triangles and filled circles are obtained from the data shown in Fig.(2.21) and Fig.(2.23) respectively.

We compare the birefringence and dielectric data shown in Fig.(2.23) and Fig.(2.24). It is noticed from Fig.(2.23) that Δn is zero in the paranematic phase. At T_{PN}, Δn rises sharply from zero value. As we have discussed in section 2.2.5, the field induced paranematic phase is uniaxial negative with the optic axis lying along the field direction. The direction of the laser beam is also parallel to the optic axis, and no optical path difference is measured along this direction.(see Fig.(2.11)). In the N_B phase, along with the field direction there is another axis, which is the direction of alignment of rods favored by the surface treatment. This is parallel to the glass plates and perpendicular to the field direction (see Fig.(2.8)). This creates the biaxiality of the medium. However, the principal director lies along the easy axis on the plates. Therefore when the transmitted intensity is measured continuously across the paranematic-nematic transition region, it shows a sharp rise from zero value. In the nematic phase, for example at 59.6 ^{0}C (see Fig.(2.23)) the enhancement in Δn is measurable up to ~325 esu. Beyond that the curves in the nematic phase are crowded though they are well separated in the transition region. Visual observations of the sample were made between crossed polarisers in the nematic phase with the principal director oriented parallel to the lower polariser (see Fig.(2.11)).

Up to a field of ~350 esu, the field of view is uniformly dark. Beyond ~350 esu some birefringent regions are seen along with the motion of the some dust particles. In spite of using a guard ring there may be a field gradient at the edges of the sample. The field may also be nonuniform inside the cell due to slight variations of the local thickness or the presence of the dust particles in the sample. Such field gradients across the sample can cause physical motion of the medium. As a result the sample can get misaligned and lead to light transmission. The merging of the curves beyond ~350 esu probably occurs due to such a misalignment.

From the dielectric data (shown in Fig.(2.24)) several important points can be noted: (i) with increasing field (a) $\varepsilon_\perp$ is increased in the N_U^- phase (for example at 60.1 ^{0}C) (b) the N_U^--N_B transition occurs at a higher temperature (c) the jump in $\varepsilon_\perp$ across the transition decreases and (d) just below the transition temperature (for example at 59.65 ^{0}C) $\varepsilon_\perp$ increases but at a lower temperature, say 59.4 ^{0}C, the curves overlap (ii) variation of $\varepsilon_\perp$ is not as sharp as that of Δn (iii) at the immediate left of the dotted line (which connects the temperatures where Δn starts to rise from zero value) the data points lie farther apart and the variation of $\varepsilon_\perp$ is faster than that on the right side. With increasing field in the paranematic phase the field induced order parameter increases and hence $\varepsilon_\perp$ is increased. We can calculate the uniaxial negative order parameter in the paranematic phase from the dielectric data, which will be discussed later. The variation of $\varepsilon_\perp$ is not as sharp as that of Δn in the transition region. This may be attributed to the fact that Δn is measured in the middle of the sample over a very small area ~10^{-3} cm^2 (diameter of the laser beam < 0.5mm) whereas $\varepsilon_\perp$ is measured over an area of ~0.2cm^2. The field as well as temperature are more uniform over the smaller region sensed in the optical study. Therefore the variations of Δn as functions of field and temperature better reflect the variation of order parameter than the dielectric data.

The orientational order parameter for uniaxial nematic liquid crystals can be well approximated by [8,17]

$$S \approx \frac{\Delta n}{\Delta n_0}. \qquad (2.47)$$

The compound used shows a very small Δn, and hence the internal field corrections are negligible. Thus it is a legitimate approximation to calculate the order parameter directly from Δn data.

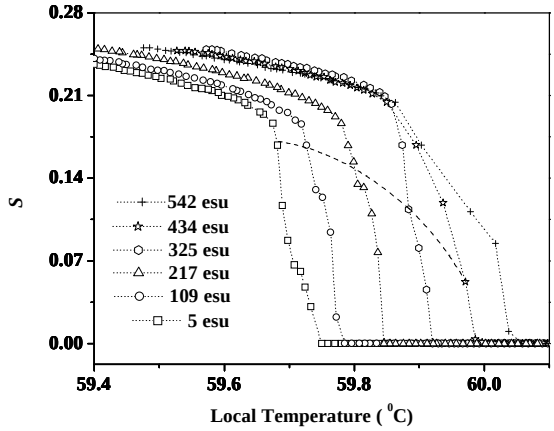

Figure 2.27: Variation of order parameter calculated (using $S=\Delta n/\Delta n_0$) from the data shown in Fig.(2.23). Dashed line connects the temperatures below which the order parameter varies smoothly.

In the nematic phase under an electric field (with $\Delta\varepsilon < 0$) the director fluctuations in the plane containing the field are reduced compared to those in the orthogonal plane. As a result the system becomes biaxial, which is described by the order parameter S ($=1.5x$, section 2.2.5) and the biaxial order parameter P. In our experiment we actually measure the birefringence in the plane orthogonal to the electric field. This is a measure of (S-P) rather than S. However, the field induced biaxial order parameter $P \sim 10^{-3}$ (at ~100 esu) in a similar sample [14] whereas $S \sim 0.2$. Hence we use Δn as a measure of the order parameter S. The variations of calculated order parameter using the equation (2.47) at various fields are shown in Fig.(2.27).

The Landau de Gennes theory (see equation (2.14)) gives rise to the following form of the temperature dependence of the order parameter in the field free uniaxial nematic liquid crystal:

$$S - S_0 = \alpha\left(1 - \frac{T}{T^{**}}\right)^{\beta} \tag{2.48}$$

where T^{**} is the absolute limit of superheating of the nematic phase, S_0 is the order

parameter at T^{**} and $\beta = 0.5$, and α is a proportionality constant. The experimental data over the entire nematic range are fitted to the above form with $S_0 = 0$ gives $\beta \approx 0.23$ (see Fig.(2.17)). This value of β is obtained in several other nematics, and the origin of this discrepancy from the measured value in not yet understood [11]. For example the predicted value of the order parameter at T^* is equal to 1.5 S_{NI} but the experimentally measured values are always much lower ($\sim 1.1\ S_{NI}$).

According to the Landau de Gennes theory (using equations (2.17) and (2.18))

$$T^{**} = T_{NI} + \frac{B^2}{36aC} \quad \text{and} \quad T^* = T_{NI} - \frac{2B^2}{9aC}. \tag{2.49}$$

It is seen that T^{**} is much closer to T_{NI} than T^*. Experiments show that $T^* \sim T_{NI} - 1^0$. Thus T^{**} is ~0.1^0 above T_{NI}, according to equation (2.49).

In order to estimate the paranematic to nematic transition temperatures from the temperature variation of the order parameter, we assume that equation (2.48) also holds good even in the presence of the field. We use the data in the nematic phase within only $0.15\ ^0$C from the transition point in this analysis.

As we have mentioned there is some misalignment of the sample beyond ~350 esu and hence we will consider the order parameter data only up to 325 esu. In Fig.(2.28) experimental values of the order parameter in the nematic phase within 0.15^0C from the transition point as well as the calculated variations using equation(2.48) are shown. The comparison between the two is reasonably good up to 217 esu, and not so good for 325 esu. The fitted values of S_0, α, β and T^{**} are shown in table-II. T^{**} is also indicated in Fig.(2.28) by vertical dotted lines. The values of T_{PN} which are defined as the temperature below which the birefringence becomes nonzero (see Fig.(2.27)) are also shown in table-II to compare with T^{**}. From table-II it is seen that at all fields T^{**} is ~$0.05\ ^0$C lower than T_{PN}. This small difference between T^{**} and T_{PN} probably arises due to the surface induced order, which will be discussed in the next section.

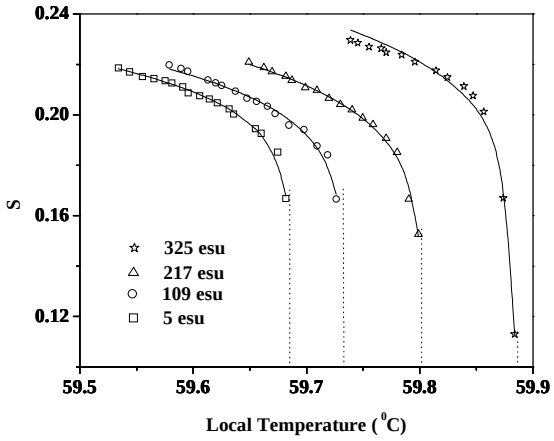

Figure 2.28: Variation of order parameter in the nematic phase within 0.15 ^{0}C of the transition point. Data points are those below the temperatures limited by the dashed line shown in Fig.(2.27). Continuous lines are the theoretical fits to the equation (2.48). Dotted vertical lines indicate the temperatures corresponding to calculated values of T^{**} (Table-II).

Table-II

Field in esu	S_0	α	β	T^{**} (^{0}C)	T_{PN} (^{0}C)
5	0.12	0.37	0.17	59.68	59.75
109	0.11	0.40	0.17	59.73	59.78
217	0.09	0.47	0.17	59.80	59.86
325	0.08	0.52	0.16	59.88	59.92

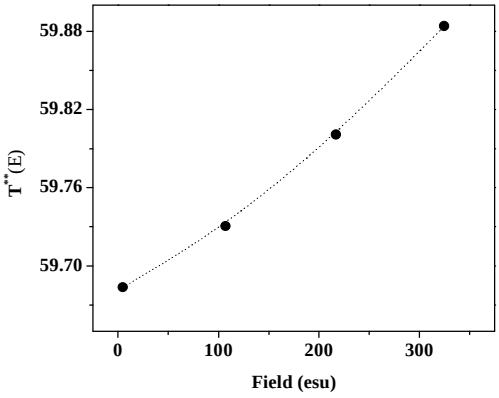

Figure 2.29: Variation of T^{**} (taken from Table-II) is shown as a function of field. Dotted line is drawn as a guide to the eye.

It is noticed (Table-II) that when the field is increased from 5 to 325 esu, S_0 decreases from 0.12 to 0.08 as expected and β decreases slightly from 0.17 to 0.16. T^{**} is plotted in Fig.(2.29) as a function of field. The amount of shift in T^{**} is ~ 0.2 ^{0}C which is similar to the shift of T_{PN} when the field is increased from 5 to 325 esu. The variation of T^{**} has both linear and quadratic dependences on the field as seen from Fig.(2.29).

2.3.2 Surface Induced Order

It is noticed from Table-II that T^{**} is ~0.05 ^{0}C lower than T_{PN} at all fields, which is defined as the temperature below which the birefringence becomes non zero. Several data points have been obtained between T^{**} and T_{PN} at 5 esu, which is practically a negligible field. At higher fields (Fig.(2.27)) the data points become more scarce as S_0 decreases. Therefore we will only discuss the order parameter data between T^{**} and T_{PN} for sample under 5 esu. In Fig.(2.30) the variation of S between T^{**} and T_{PN} is shown on an expanded scale.

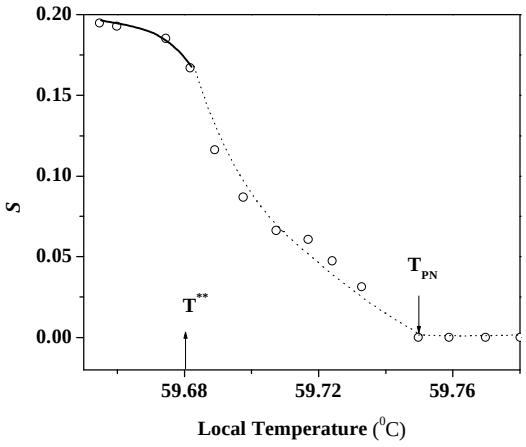

Figure 2.30: Variation of order parameter at a field of 5 esu. Here a small portion (59.67 ^{0}C to 59.78 ^{0}C) of the curve (shown in Fig.(2.27)) is expanded. Vertical up and down arrows denote T^{**} and T_{PN} respectively (Table-II). Note the curvature of the solid line below T^{**} is opposite to the curvature of the dotted line above T^{**}.

It is noticed that below 59.68 ^{0}C, the order parameter *S* follows the temperature variation given by equation (2.48) and above this temperature the curvature changes sign. The change of curvature is better seen at the lowest field (~5esu) than at higher fields and is also seen in independent experiments (see Fig.(2.25)). The measurements are made on cooling the sample from the higher temperature phase. The SiO coating provides a strong anchoring at the surface, aligning the molecules along the easy direction. The surface alignment is expected to be retained even in the higher temperature phase.

There are several experimental and theoretical studies on the influence of the surface order on the nematic –isotropic transition [19-23]. Using the Landau de Gennes theory Ping Sheng [20] showed that if the order parameter at the surface is higher than that in the bulk, the transition at the surface occurs at a higher temperature than in the bulk. A higher order parameter at the surface is expected to arise from the interactions between confining surfaces and the liquid crystal molecules. Experimentally Miyano [21] measured the wall-induced birefringence above the isotropic-nematic phase transition point. He showed that the pretransitional birefringence measured in the homeotropic geometry of the sample diverges as T_{NI} is approached from the isotropic phase. In a light scattering experiment Mada et al [22] reported that the bulk isotropic –nematic transition occurs at ~0.1^{0}C below that at the surface. Using a density functional theory of nematic liquid crystals Selinger et al [23] predicted a complete wetting near the free surfaces of a nematic arising from a strong surface field (V_S =10V_0 , where V_0 is the Maier-Saupe orientation potential between the molecules). The profile of the calculated order parameter is reproduced in Fig.(2.31). Because of the assumed strong surface field, $\langle P_2(\cos\theta)\rangle$ is saturated at the surface. At temperatures above T_{NI} , away from the surface it quickly decays to a value close to the Maier-Saupe bulk nematic value of 0.429 at the N-I transition point. This value is retained for a certain length before the order parameter decays to the bulk isotropic value of 0. The distance over which $\langle P_2(\cos\theta)\rangle$ = 0.429 increases as $|\ln t|$ as $t \to 0^+$, where $t = (T - T_{NI})/T_{NI}$ is the reduced temperature. This increase is reflected in the effective nematic order parameter, integrated over the thickness, $\Gamma(t)$, which also diverges logarithmically with *t* (Fig.(2.32)). Though these calculations have been made for homeoptropic alignment, the results for homogeneous

alignment are expected to be similar, as has been found on the basis of the Landau- de Gennes theory by Ping Sheng [20].

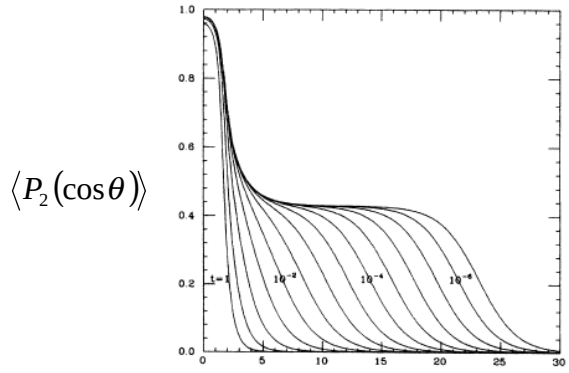

Figure 2.31: Profile of order parameter $\langle P_2(\cos\theta)\rangle$ showing nematic order near a free surface for reduced temperature $t=(T-T_{NI})/T_{NI}=10^{0},10^{-0.5},....,10^{-6.5}$. (adapted from ref.[23]). (r_0 is approximately the radius of the cylindrical molecule)

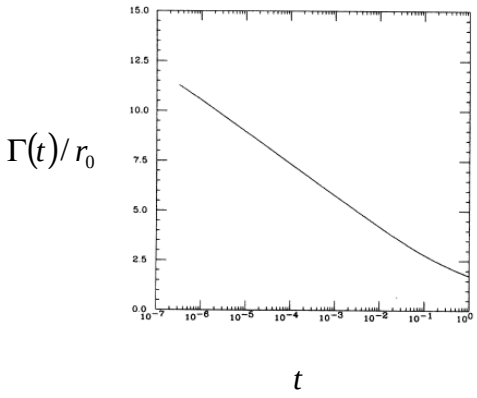

Figure 2.32: The calculated integrated nematic order parameter $\Gamma=\int_0^{\infty}\langle P_2(\cos\theta)\rangle dz$ as a function of the reduced temperature $t=(T-T_{NI})/T_{NI}$ (adapted from ref.[23])

In Fig.(2.33) we show the variation of measured order parameter (S) with the reduced temperature τ $\left(=(T-T^{**})/T^{**}\right)$ between T^{**} and T_{PN} . In this small temperature range S diverges logarithmically. Therefore we believe that this part of the curve

represents the surface induced order before the bulk transition takes place at T^{**}, which is practically indistinguishable from the bulk transition temperature.

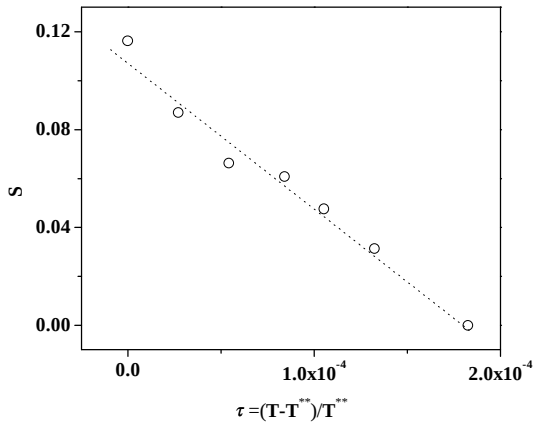

Figure 2.33: Variation of order parameter as a function of reduced temperature (τ). Dotted line is drawn as a guide to the eye.

2.3.3 Order Parameter Enhancement by the Field

In this section we compare the enhancement of order parameter with the theoretical predictions described in sections 2.2.4 and 2.2.5. It is convenient to use the birefringence data shown in Fig.(2.25) because the data points are available down to ~59.4 ^{0}C. Analysis is carried out up to 334 esu because beyond that the sample gets misaligned as discussed in the last section. The variation of enhanced order parameter as a function of field at several temperatures is shown in Fig.(2.34).

The increase in order parameter due to the application of electric field arises because of two physical mechanisms. One mechanism is the macroscopic quenching of thermal fluctuations of the director as discussed in section 2.2.4 (equation (2.31)). The enhancement of order parameter for a system with $\Delta\varepsilon < 0$ due to this effect alone can be written as [15]

$$\delta S_l = S(E,T) - S(0,T) = \frac{3k_B T}{8\pi (K)^{3/2}} \left(\frac{\Delta\varepsilon}{4\pi} \right)^{1/2} |E| \qquad (2.50)$$

$$= c_l |E|$$

where K is the average curvature elastic constant, $S(E,T)$ is order parameter in the presence of field and $S(0,T)$ is the same in the absence of field. The subscript l indicates a linear variation with $|E|$.

Another mechanism for the enhancement of order parameter under the application of field is the Kerr effect, which is microscopic in origin as discussed in section 2.2.5. The increase in order parameter due to this effect alone can be written as

$$\delta S_q = c_q E^2 \tag{2.51}$$

where c_q is an appropriate susceptibility. This effect is *quadratic* in E, indicated by the subscript q. The enhancement in the order parameter due to both the effects can be written as

$$\delta S(E) = \delta S_l + \delta S_q = c_l |E| + c_q E^2 . \tag{2.52}$$

The variation of measured δS $(= S(E) - S(0))$ at different temperatures is shown in Fig.(2.34). Using a least squares fitting procedure, the enhancement of the order parameter is fitted with the equation (2.52).

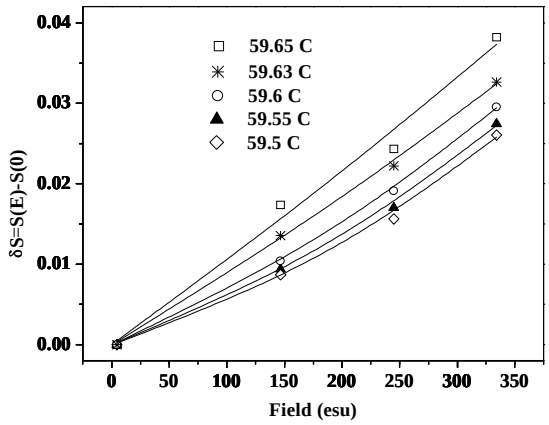

Figure 2.34: Variation of enhancement of the order parameter (δS) as a function of field at different local temperatures. Continuous lines are fit to the functional form of $\delta S = c_l |E| + c_q E^2$.

It is noticed from Fig.(2.34) that at higher temperatures (closer to the transition point, for example at 59.65 ^{0}C) the variation of δS is nearly linear and the quadratic

effect is seen at higher fields as the temperature is lowered. The temperature variation of the fitted parameters c_l and c_q are shown in Fig.(2.35). c_l decreases and c_q increases as the temperature is lowered in the nematic phase. In a mean-field model $K \propto S^2$ and $\Delta\varepsilon \propto S$,

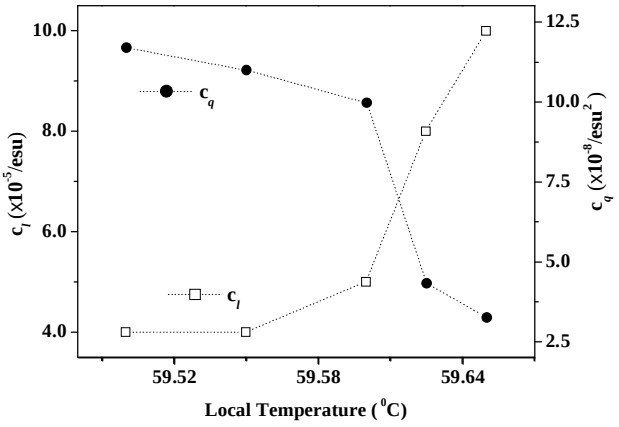

Figure 2.35: Variations of the fitted parameters c_l and c_q are shown as functions of local temperature. Dotted lines are drawn as guides to the eye.

therefore the susceptibility c_l decreases rapidly ($c_l \sim S^{-2.5}$) as the temperature is lowered in the nematic phase. On the other hand c_q is proportional to the $\Delta\varepsilon$, which increases as the temperature is lowered in the nematic phase.

We have also calculated the uniaxial negative order parameter (S_{U^-}) from the dielectric constant data taken from Fig.(2.24). In the paranematic phase the field-induced director i.e the symmetry axis is parallel to the field. Thus the measurement yields $\varepsilon_{\parallel}^{P}$ which is given by $\varepsilon_{\parallel}^{P} = \bar{\varepsilon} + \frac{2}{3}\Delta\varepsilon_0 S_{U^-}$ where S_{U^-} is the negative uniaxial order parameter as $\Delta\varepsilon_0$ is negative. In the nematic phase the principal director is perpendicular to the field and we measure $\varepsilon_{\perp}^{N}$ which is given by $\varepsilon_{\perp}^{N} = \bar{\varepsilon} - \frac{1}{3}\Delta\varepsilon_0 S$ (ignoring biaxiality which is very small). We have used the value of S obtained by optical measurement at $(T_{PN}$ -2)^{0}C to evaluate $\Delta\varepsilon_0$ (= -9.97). Above the tricritical point the paranematic-nematic transition is second order and, $\varepsilon_{\parallel}^{P} = \varepsilon_{\perp}^{N}$ and hence it is expected that $S_{U^-} = -\frac{1}{2}S$ at T_{PN}.

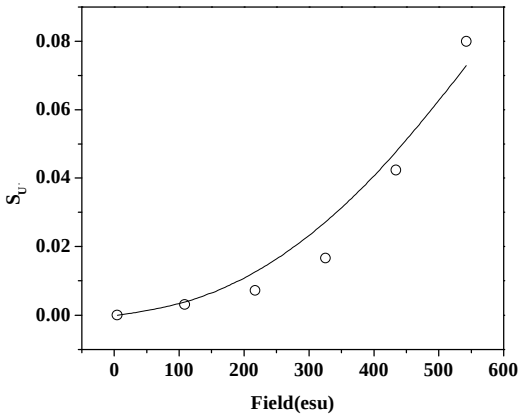

Figure 2.36: Variation of uniaxial negative order parameter (S_{U^-}) in the paranematic phase as a function of applied field at a temperature 60.1 ^{0}C. Points are experimental data. Continuous line is the fit to the functional form $S_{U^-} = c_q E^2$, where c_q=2.5×10^{-7} cgs units.

The variation of uniaxial order parameter S_{U^-} is shown as a function of the applied field in Fig.(2.36). A least squares fitting procedure is used to fit the data with the equation $S_{U^-} = c_q E^2$. The agreement with the measured data is not very good. As we discussed earlier the dielectric data is measured over a large area ($0.2cm^2$) and the field and temperature may not be uniform in the cell.

The enhancement of order parameter near the surface, which was discussed in the last section, also contributes to $\varepsilon_{\parallel}^{P}$. However it is expected that $\varepsilon_{\parallel}^{P}$ mainly arises from the field-induced order in the bulk in the paranematic phase.

2.3.4 Variation of T_{PN} with Field: Inclusion of Director Fluctuations

The paranematic-nematic transition temperature (T_{PN}) in Fig.(2.26) shows a linear dependence on the r.m.s value of the field. According to the prediction of the Landau de Gennes theory, T_{PN} varies quadratically with the field. The linear variation of T_{PN} with field indicates that the quenching of director fluctuations also influences the paranematic–nematic (P-N) transition. Below the tricritical point P-N is a first order transition with a finite jump in the order parameter at the transition point, and the fluctuations of the order parameter can be expected to be relatively small. In order to take into account the

director fluctuations on the P-N transition it is simpler to consider a system with $\Delta\varepsilon > 0$. The systems with $\Delta\varepsilon > 0$ remain uniaxial under the field and the calculation is easier. Indeed even in the systems with $\Delta\varepsilon > 0$, ΔT_{PN} appears to vary linearly with field (see Fig.(2.6)).

The entropy of the system is reduced due to the quenching of the director fluctuations by the field and as a result the free energy increases. We may point out an analogous problem of the undulation interaction, which arises in lamellar systems. In this case, the layer fluctuations are restricted due to the presence of the neighboring layers and the corresponding increase in the free energy was calculated by Helfrich [24]. In the case of nematic liquid crystals the director fluctuation amplitude is reduced in the presence of the field but the number of fluctuation modes remains unaltered. We can use a dimensional analysis to estimate the corresponding increase in the free energy density. As we have mentioned in section 2.2.4, there are two length scales in this problem. One is the electric coherence length $\xi(E) = \left(\frac{K}{\Delta\varepsilon / 4\pi} \right)^{1/2} \frac{1}{|E|}$, and the other is the cut off wave vector q_c ($\approx 2\pi/a$, where a is a typical molecular dimension). As the additional contribution arises from an entropic origin, we write the free energy density with the following combinations of thermal energy $k_B T$ and the above two lengths:

$$\Delta F = k_B T \frac{q_c^2}{\xi} + k_B T \frac{q_c}{\xi^2}. \tag{2.53}$$

As $K = K_0 S^2$ and $\Delta\varepsilon = S\Delta\varepsilon_0$, we can write $\xi(E) = C \frac{\sqrt{S}}{|E|}$, where the constant $C = \left(4\pi K_0 / \Delta\varepsilon_0 \right)^{\frac{1}{2}}$. Substituting $\xi(E)$ in equation (2.53) we get

$$\Delta F = \frac{\alpha T}{\sqrt{S}} |E| + \frac{\beta T}{S} E^2 \tag{2.54}$$

where $\alpha = k_B q_c^2 / C$, and $\beta = k_B q_c / C^2$ are constants and $\beta << \alpha$. It is noticed that the above expression is non-analytic in S. However, this contribution to ΔF is zero when $E = 0$.

We can justify the above form of ΔF by the following physical argument: We can treat the director fluctuation as a random variable [11]. The fluctuation amplitude can be assumed to have the Gaussian distribution

$$W(n_\perp) = \frac{2}{C'\sqrt{2\pi\langle n_\perp^2\rangle}} Exp\left(-\frac{n_\perp^2}{2\langle n_\perp^2\rangle}\right) \tag{2.55}$$

where C' is a normalizing constant and it can be found by normalizing $W(n_\perp)$ i.e

$$\int_0^1 W(n_\perp)\, dn_\perp = 1. \tag{2.56}$$

It should be pointed out that the limit of the integration is taken from 0 to 1 instead of 0 to infinity as for a usual Gaussian distribution. In the absence of the field the fluctuation amplitude is given by $\langle n_\perp^2\rangle_0 = (k_B T / 2\pi^2 K) q_c$ (equation (2.29)). We estimated $\langle n_\perp^2\rangle_0$ ~0.14 in the nematic phase at 50 ^{0}C, assuming the cut off wave vector $q_c \approx 2\pi/a$, where $a \sim 10\ \overset{0}{A}$, and elastic constant K~5×10^{-7} dynes. For this value of $\langle n_\perp^2\rangle_0$, 95% of the area of the variation of $W(n_\perp)$ is covered within $n_\perp \sim 0.8$ and hence the upper limit of integration can be taken to be infinity and the normalising constant is then $C' \approx 1$. With increasing field $\langle n_\perp^2\rangle_E$ decreases and hence the approximation is more justifiable. The entropy due to this distribution is given by

$$\zeta = -k_B \int_0^1 W(n_\perp)\ \ln(W(n_\perp))\ dn_\perp . \tag{2.57}$$

Which can be simplified as

$$\zeta = -k_B\left[-\frac{1}{2} + \ln\left(\frac{2}{\sqrt{2\pi\langle n_\perp^2\rangle}}\right)\right]. \tag{2.58}$$

The difference in entropies in the presence of field and in the absence of field is given by

$$\Delta\zeta = \zeta_E - \zeta_0 = -k_B\left[\ln\left(\sqrt{\langle n_\perp^2\rangle_0}\right) - \ln\left(\sqrt{\langle n_\perp^2\rangle_E}\right)\right] \tag{2.59}$$

where ζ_E and ζ_0 are the entropies and $\langle n_\perp^2 \rangle_E$ and $\langle n_\perp^2 \rangle_0$ are the mean square director fluctuations in the presence and in the absence of electric field respectively. From equation (2.28),

$$\langle n_\perp^2 \rangle_E = \frac{k_B T}{2\pi^2 K}\left(q_c - \frac{1}{\xi}\left(\frac{\pi}{2} - \frac{1}{q_c \xi} \right) \right) \tag{2.60a}$$

and

$$\langle n_\perp^2 \rangle_0 = \frac{k_B T}{2\pi^2 K} q_c \,. \tag{2.60b}$$

The excess free energy is given by $\Delta F = -T\Delta\zeta$. Using equations (2.59), (260a) and (2.60b) the simplified form of the free energy can be written as

$$\Delta F = \frac{\alpha' T}{\sqrt{S}}|E| + \frac{\beta' T}{S} E^2 \tag{2.61}$$

where α' and β' are two constants and related to the cut off wave vector q_c. The form of equation (2.61) is similar to that of equation (2.54).

Now the total free energy density in the nematic phase can be written as

$$F_N(p,T,S) = F_0(p,T) - GSE^2 + \frac{a(T-T^*)}{2}S^2 - \frac{B}{3}S^3 + \frac{C}{4}S^4 + T\left[\frac{\alpha|E|}{\sqrt{S}} + \frac{\beta E^2}{S}\right] \tag{2.62}$$

where $G = \Delta\varepsilon_0 / 12\pi$. Close to the critical point $\langle n_\perp^2 \rangle$ can be large and the above approximation is no more valid and further the order parameter fluctuation should be taken into account. In the paranematic phase there is no director in the absence of field and hence the free energy density in the paranematic phase is given by

$$F_P(p,T,S) = F_0(p,T) - GSE^2 + \frac{a(T-T^*)}{2}S^2 - \frac{B}{3}S^3 + \frac{C}{4}S^4 \,. \tag{2.63}$$

The paranematic to nematic transition temperature is found numerically by comparing the above two energies (F_N and F_P). For illustration we use the Landau coefficients which are known for 5CB [3] a = 0.13 *J*/cm^3-*K*, B = 1.6 *J/cm*^{3}, C = 3.9 *J/cm*^{3}, T_{NI} = 306.8 *K* and G = 0.55. The parameters α and β are estimated to be ~0.01 and 0.00001 respectively. We find that the paranematic-nematic transition temperature shows practically a linear variation up to 100 esu and beyond that the influence of the quadratic component is seen. (Fig.(2.37)). In the case of a system with $\Delta\varepsilon < 0$, the biaxial order has to be taken in to

account, which is not considered in the present calculation. However from dimensional argument the basic form of the contribution to free energy density should be the same. This variation can be compared with the variation of T^{**} under the field which was found by fitting the order parameter at various fields (Fig.(2.29)).

The field dependence of the order parameter in the nematic phase is calculated by minimising the free energy F_N given by equation (2.62). The variation of order parameter as a function of field at $T_{PN} - 0.1^0$ is shown in Fig.(2.38). We see that the calculated variation of order parameter in the nematic phase has a trend similar to that of the measured variation as shown in Fig.(2.34).

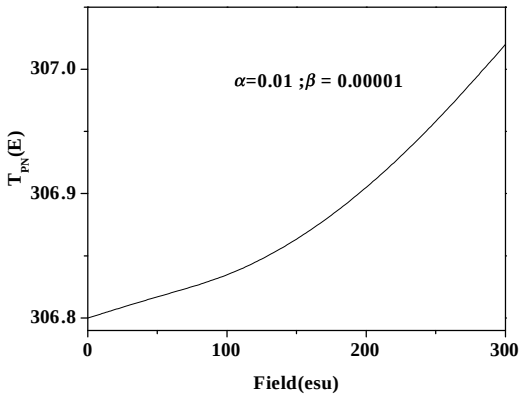

Figure 2.37: Variation of calculated T_{PN} as a function of electric field.

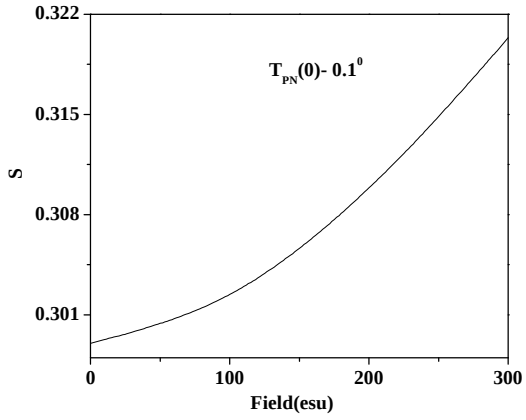

Figure 2.38: Variation of order parameter in the nematic phase at T_{PN}-0.1^0 as a function of field.

2.3.5 Order Parameter Susceptibility: Generation of third harmonic component of the electrical signal

In this section we discuss the order parameter susceptibility. In the case of magnetism, the susceptibility is defined as $\chi = \partial M / \partial H$, where the magnetic field *H* is conjugate to the magnetisation. Similarly the order parameter *S* which is a second rank tensor, is conjugate to E^2. The orientation dependent part of dielectric energy denoted by $-\frac{\Delta\varepsilon}{8\pi}\left(\hat{n}.\vec{E}\right)^2$ and $\Delta\varepsilon \propto S$. The order parameter susceptibility can be defined as

$$\chi_q = \frac{\partial S}{\partial E^2} \tag{2.64}$$

where $\delta S(E) = S(E) - S(0)$. In order to get an experimental measurement of χ_q, we calculate the current flowing through the cell. The sample capacitance is given by

$$C_S = C_0 \varepsilon_\perp \tag{2.65}$$

where C_0 is the capacitance of the empty cell and $\varepsilon_\perp = \bar{\varepsilon} - \frac{1}{3}\Delta\varepsilon_0 S(E)$. Using equation (2.64) and (2.65) we get

$$C_S = C_0\left(\bar{\varepsilon} - \frac{1}{3}\Delta\varepsilon_0 S(E)\right) = C_1 - C_q E^2 \tag{2.66}$$

where $C_1 = C_0\left(\bar{\varepsilon} - \frac{1}{3}\Delta\varepsilon_0 S(0)\right)$,

and $C_q = \frac{1}{3}\Delta\varepsilon_0 C_0 \chi_q$. (2.67)

From C_q we can measure χ_q. The applied voltage to the cell is given by $V = V_0 \sin\omega t$ where $\omega = 2\pi f$, f being the frequency. The corresponding field is given by $E = V/d$, where *d* is the cell thickness. Considering only the capacitive response the current through the cell is given by

$$I = \frac{d}{dt}[C_S V] = \frac{d}{dt}[C_S E d]. \tag{2.68}$$

Using equations (2.66) and (2.67) we get

$$I = \frac{d}{dt}\left[\left(C_1 - C_q E^2\right)E\right] d$$

$$= \omega\left[C_1 V_0 \cos\omega t - \frac{3C_q V_0^3}{4d^2}\left(\cos\omega t - \cos 3\omega t\right)\right]. \tag{2.69}$$

The magnitude of third harmonic component of the current is given by

$$I_{3\omega} = \left(\frac{3C_q V_0^3}{4d^2}\right)\omega \ . \tag{2.70}$$

Using this equation we can measure C_q. From measured C_q we can get χ_q using equation (2.67) .

Thus, the quadratic dependence of the enhancement of order parameter on the electric field leads to generation of third harmonic signal [6]. The measured voltage across the capacitor C_m (see Fig.(2.11) corresponding to the third harmonic current is given by

$$V_{3\omega} = I_{3\omega} Z = \frac{I_{3\omega}}{\omega C_m} \tag{2.71}$$

$$= \frac{3C_q V_0^3}{4d^2 C_m}. \tag{2.72}$$

Therefore χ_q is given by

$$\chi_q = \left[\frac{4C_m d^2}{\Delta\varepsilon_0 C_0 V_0^3}\right] V_{3\omega}. \tag{2.73}$$

By measuring the third harmonic component of electric signal we can measure electric susceptibility of the order parameter.

As we discussed earlier an important contribution to $\delta S(E)$ in the nematic phase comes from the quenching of director fluctuations. This enhancement is proportional to $|E|$ and the relevant order parameter susceptibility can be defined as

$$\chi_l = \frac{\partial S}{\partial |E|}. \tag{2.74}$$

The Fourier components of $|E|$ are given by

$$|E| = |E_0 \sin\omega t| = \frac{2}{\pi} E_0\left(1 - \frac{2}{3}\cos 2\omega t - \frac{2}{15}\cos 4\omega t + ...\right).$$

The component at 2ω in $|E|$ gives rise to the susceptibility

$$\chi_l = \frac{3\pi\, d}{2}\left(\frac{C_m}{\Delta\varepsilon_0 C_0 V_0^2}\right)V_{3\omega}. \qquad (2.75)$$

Thus, in the nematic phase the measured third harmonic signal $V_{3\omega}$ has contributions from both the quenching of director fluctuations as well as from Kerr effect. It is noticed from equations (2.73) and (2.75) that $\chi_q \propto V_{3\omega}/V_0^3$ and $\chi_l \propto V_{3\omega}/V_0^2$, where V_0 is the amplitude of the applied voltage.

We have simultaneously measured the first (f), second (2f) and third (3f) harmonic electrical signals as well as the transmitted intensity as functions of local temperature near the paranematic-nematic transition point at relatively high fields. Variations of the third harmonic electrical signals (3f) as functions of local temperature, measured at two different fields namely 430 esu and 537 esu at a frequency of 1111 Hz are shown in Fig.(2.39). As we mentioned earlier, there is some misalignment of the director above 350 esu. However, this does not affect the electrical measurements which essentially sense only $\varepsilon_\perp$ at even high fields. The 3f signal at 430 esu shows a nearly symmetric narrow peak at 59.89 ^{0}C. Its value at the peak (~2.8×10^{-4}V) is ~ 6 times larger than that of the background signal. The temperature at which the peak occurs corresponds to the paranematic-nematic transition temperature (T_{PN}). At 537 esu the peak occurs at a

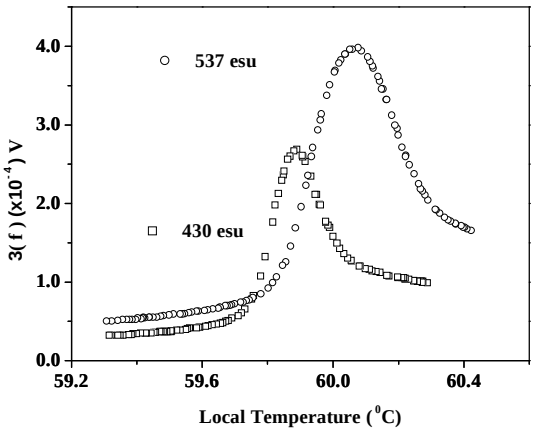

Figure 2.39: Variations of the third harmonic electrical (3f) signals as functions of local temperature. Cell thickness: 15.5 μm, applied field: 537 esu (open circles) and 430 esu (open squares), Frequency: 1111 Hz.

higher temperature (60.08 ^{0}C). The signal at the peak (~ 4×10^{-4} V) measured at 537 esu is ~ 8 times larger than the background signal.

We have evaluated $V_{3\omega}/V_0^2$ and $V_{3\omega}/V_0^3$ at two temperatures (Table-III). When the temperature is below 59.6 ^{0}C i.e sufficiently far away from T_{PN} (see Fig.(2.39)) it is easier to measure the relevant parts, and the former ratio is a constant while the latter is not. It indicates that at the temperatures near T_{PN} the main contribution to the order parameter susceptibility comes from the quenching of director fluctuations.

Table-III

Temperature (^{0}C)	$V_{3\omega}/V_0^3$		$V_{3\omega}/V_0^2$	
	$V_0 = 200$ V	$V_0 = 250$ V	$V_0 = 200$ V	$V_0 = 250$ V
59.4	4.3×10^{-12}	3.4×10^{-12}	8.5×10^{-10}	8.4×10^{-10}
59.6	5.5×10^{-12}	4.1×10^{-12}	1.1×10^{-9}	1.0×10^{-9}

We show the variations of the 3f signal as well as the transmitted intensity in Fig.(2.40) as functions of local temperature.

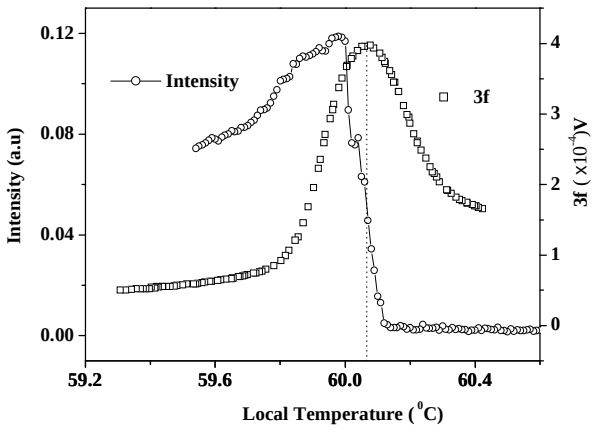

Figure 2.40: Variations of transmitted intensity as well as the third harmonic electrical signal as functions of local temperature: Dotted vertical line denotes the P-N transition temperature corresponding to the peak in the 3f signal. Cell thickness: 15.5 μm, applied field: 537esu, Frequency: 1111 Hz.

The temperature at which 3f signal shows a peak (60.08 ^{0}C) is indicated by a dotted line (see Fig.(2.40)). It occurs at a slightly lower temperature (~ 0.05 ^{0}C) than the temperature (60.13 ^{0}C) at which the transmitted intensity rises from zero value.

Under a strong electric field the P-N transition becomes second order. In the case of strongly polar compounds it is possible that the dipole moments of the molecules may get correlated over large domains. Due to the slow dynamics near the tricritical point the domains may not be able to reorient at the frequency of the applied field. As a result a second harmonic electrical signal (2f) can be generated [6]. Since the compound used by us is also highly polar we looked for 2f electrical signal under strong field. The variation of measured 2f component of the electrical signal across the paranematic-nematic transition is shown in Fig.(2.41). It has some background due to the nonlinearity of the voltage amplifier. However near the P-N transition point a small peak in 2f signal which is ~20% higher than the background is seen and it occurs at the same temperature as that of the peak in the 3f component (Fig.(2.41)). It may indicate the presence of polarized domains that do not reorient with the field [6].

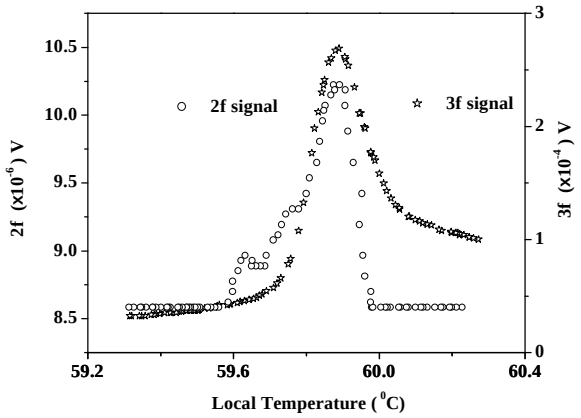

Figure 2.41: Variations of third (3f) and second (2f) harmonic electrical signals across the paranematic-nematic transition region as a function of local temperature. Cell thickness: 15.5 μm, applied field: 430 esu, frequency: 1111 Hz.

2.4 Conclusions

We have performed the first high electric field experiment on a nematic liquid crystal with $\Delta\varepsilon < 0$. The local temperature measurement clearly shows that the

paranematic to nematic transition temperature (T_{PN}) varies linearly with $|E|$ which indicates that the director fluctuations contribute to the thermodynamics of the phase transition. As we could not perform optical measurements beyond 350 esu, we are unable to precisely locate the tricritical point. However, the electrical measurements shows a peak in the third harmonic signal which clearly indicates that the transition has become second order beyond about 350 esu.

References

[1] W. Helfrich, "Effect of electric fields on the temperature of phase transitions of liquid crystal.," Phys. Rev. Lett. **24**, 201 (1970).

[2] A. J. Nicasto and P. H. Keyes, "Electric field induced critical phenomena at the nematic-isotropic transition and the nematic-isotropic critical point.," Phys. Rev, A, **30**, 3156 (1984).

[3] L. Lelidis and G. Durand, "Electric-field-induced isotropic-nematic phase transition.," Phys. Rev. E, **48**, 3822 (1993).

[4] L. Lelidis, M. Nobili and G. Durand, "Electric field-induced change of the order parameter in the nematic liquid crystals.," Phys. Rev. E, **48**, 3818 (1993).

[5] G. Bassapa and N. V. Madhusudana, "Effect of strong electric fields on the phase transitions in some liquid crystals.," Mol. Cryst. Liq. Cryst. **288**, 161 (1996).

[6] G. Basappa and N.V. Madhusudana, "Effect of strong electric field on a nematogen: evidence for polar short range order.," J. Eur. Phys. B, **1**, 179 (1998).

[7] C. Rosenblatt, "Magnetic field dependence of the nematic-isotropic transition temperature.," Phys. Rev. A, **24**, 2236 (1981).

[8] S. Chandrasekhar, “Liquid Crystals”, 2nd ed. (Cambridge University Press, 1992).

[9] L. D. Landau and E. M. Lifshitz, Statiscal Phys. 3rd part1 ed. (Pergamon Press,1980).

[10] E. F. Grasmbergen, L. Longa and W.H. de Jeu, “Landau theory of the isotropic-nematic phase transitions.,” Phys. Rep. **135**, 195 (1986).

[11] P. G. de Gennes, and J. Prost, “The physics of liquid crystals.,” (Clarendon Press, Oxford, 1995).

[12] B. Malraison, Y. Poggi and E. Guyon, “Nematic liquid crystals in high magnetic field: Quenching of the transverse fluctuations.,” Phys. Rev. A, **21**, 1012 (1980).

[13] C. Fan and M. J. Stephen, “Isotropic-nematic phase transition in liquid crystals.,” Phys. Rev. Lett. **25**, 500 (1970).

[14] D. A. Dunmur, K. Szumilin and T. F. Waterworth, “ Field induced biaxiality in nematics.,” Mol. Cryst. Liq. Cryst. **149**, 385 (1986).

[15] D. A. Dunmur, K. Szumilin, “ Field quenching of director fluctuations in thin films of nematic liquid crystals.,” Liq. Cryst. **6**, 449 (1989). P. P Muhoray, D. A. Dunmur, “Field–induced order in nematic liquid crystals.,” Mol. Cryst. Liq. Cryst. **97**, 337 (1983).

[16] I. Haller, H. A. Huggins, H. R. Lilienthal, T. R. McGuire, “Order-related properties of some nematic liquids., ”, J. Phys. Chem. (USA) **77**, 950 (1973).

[17] D. A. Dunmur, A. Fukuda and G. R. Luckhurst, “Liquid Crystals: Nematics.,” (An Inspec Publication), pp-271.

[18] Z. Li, O. D. Lavrentovich, “ Surface anchoring and growth pattern of the field-driven first order transition in a smectic-A liquid crystal.,” Phys. Rev. Lett. **73**, 280 (1994).

[19] M. I. Boamfa, M. W. Kim, J. C. Maan and T. Rasing. “Observation of surface and bulk phase transition in nematic liquid crystal.,” Nature **49**, 149 (2003).

[20] P. Sheng, “Boundary-layer phase transition in nematic liquid crystals.,” Phys. Rev. A, **26**, 1610 (1982).

[21] K. Miyano, “Wall-induced pretransitional birefringence: a new tool to study boundary aligning forces in liquid crystals.,” Phys. Rev. Lett. **43**, 51 (1979).

[22] H. Mada and S. Kobayashi, “ Surface and bulk order parameter of a nematic liquid crystal.,” Appl. Phys. Lett. **35**(1), 4 (1979). Y. Imura, H. Mada, S. Kobayashi, “Measurement of the phase transition of p-Heptyl-p’-cyanobiphenylin in the bulk and boundary.,” Phys. Lett. **103A**, 342 (1984).

[23] J. V. Selinger and D. R. Nelson, “Density functional theory of nematic and smectic-A order near surfaces.,” Phys. Rev. A, **37**, 1736 (1988).

[24] W. Helfrich, “Steric interaction of fluid membrane in multilayer systems.,” Z. Natruforsch, **33a**, 305 (1978).